

NOVEL RF MICROELECTROMECHANICAL SYSTEMS TUNABLE FILTERS  
WITH ADJUSTABLE SPURIOUS SUPPRESSION

A Thesis

by

VIKRAM SEKAR

Submitted to the Office of Graduate Studies of  
Texas A&M University  
in partial fulfillment of the requirements for the degree of

MASTER OF SCIENCE

December 2008

Major Subject: Electrical Engineering

NOVEL RF MICROELECTROMECHANICAL SYSTEMS TUNABLE FILTERS  
WITH ADJUSTABLE SPURIOUS SUPPRESSION

A Thesis

by

VIKRAM SEKAR

Submitted to the Office of Graduate Studies of  
Texas A&M University  
in partial fulfillment of the requirements for the degree of  
MASTER OF SCIENCE

Approved by:

Chair of Committee,	Kamran Entesari
Committee Members,	Robert D. Nevels
	Jun Zou
	Debjyoti Banerjee
Head of Department,	Costas Georghiadis

December 2008

Major Subject: Electrical Engineering

## ABSTRACT

Novel RF Microelectromechanical Systems Tunable Filters  
with Adjustable Spurious Suppression. (December 2008)  
Vikram Sekar, B.E., Visvesvariah Technological University  
Chair of Advisory Committee: Dr. Kamran Entesari

This thesis presents the theory and design of fixed and Radio Frequency (RF) Microelectromechanical Systems (MEMS) -based tunable microwave filters for RF and microwave applications. The methodology for the design of coupled resonator filters is explained in detail and is used to design an end-coupled microstrip filter at 1.5 GHz with inductive loading using a stepped microstrip discontinuity to lower the resonance frequency of the half-wavelength microstrip resonator. The fabricated end-coupled filter shows center frequencies of 1.36 GHz and 1.03 GHz in the unloaded and loaded state respectively, with insertion losses between 1.2-1.5 dB and return loss better than 10 dB in both states. The filter response shows spurious passbands at approximately twice the filter center frequencies. To overcome this problem and improve the upper rejection skirt of the filter, microstrip resonators with tapped input/output coupling and mixed inter-resonator coupling are used to suppress the spurious passband by introducing a transmission zero at spurious resonance frequency. Measurement results for the fabricated tapped-resonator filters show an improvement of the upper rejection skirt due to spurious suppression to a level of -40 dB, with insertion loss of 1.2-1.5 dB for the same center frequencies.

The concepts developed from fabrication and measurement of fixed-tuned microstrip filters are used to design an inductively-loaded RF MEMS tunable filter with adjustable spurious suppression implemented using packaged metal-contact switches. The two-pole 5% filter has a tuning range of 17% from 1.06 GHz to 1.23 GHz with an

insertion loss of 1.56-2.28 dB and return loss better than 13 dB over the tuning range. The inductive loading mechanism is used to tune the open-ended quarter wavelength stub such that a tunable transmission zero suppresses the spurious resonance as the filter center frequency is tuned. The spurious passband response in both states is suppressed below -20 dB. The unloaded quality factor (Q) of the filter varies from 127 to 75 as the filter is tuned. The equivalent circuit model for the series metal-contact packaged RF MEMS switch used in the tunable filter is derived from full-wave electromagnetic simulations and used to predict the effect of MEMS switch parasitics on the overall performance of the tunable filter.

To my family and loved ones.

## ACKNOWLEDGMENTS

Among those who contributed to my graduate studies at Texas A&M University, I would especially like to thank Prof. Kamran Entesari for guiding me through my master's program. Under his guidance, I developed scientific rigor in thought and an ethical approach to research that will be the foundation for every learning experience in the future. With his support, I have had the opportunity to understand the workings of the scientific community. I have felt motivated and encouraged to try new ideas and apply them to different scenarios in science and engineering. I would also like to thank my other committee members, Prof. Robert D. Nevels, Prof. Jun Zou and Prof. Debjyoti Banerjee for their participation, support and feedback.

I would also like to thank Dr. Kai Chang for providing fabrication facilities without which this thesis would have never been possible. I would also like to thank Mr. Mingyi Li for his patient support with all my fabrication needs. I would also like to thank Mohamed El-Nozahi for valuable technical advice regarding measurement. I would also like to thank Stephen Andrew Long and Sean Goldberger for help with the mask preparation for fabrication.

I would like to thank all my friends for their support and understanding. I would finally like to thank my family for their unconditional love and support throughout the course of my master's program which has been the greatest motivation for me to keep progressing during all these years.

## TABLE OF CONTENTS

CHAPTER		Page
I	INTRODUCTION . . . . .	1
	A. Tunable Filter Applications . . . . .	1
	B. Filter Tuning Techniques . . . . .	2
	C. Thesis Overview . . . . .	3
II	DESIGN OF INDUCTIVELY-LOADED FIXED-TUNED MICROSTRIP FILTERS . . . . .	5
	A. Introduction . . . . .	5
	B. Design . . . . .	6
	1. End-coupled microstrip filter . . . . .	9
	a. Methodology . . . . .	9
	b. Inductive resonator loading . . . . .	14
	2. Tapped resonator microstrip filter with mixed coupling	18
	a. Suppression of spurious responses . . . . .	18
	b. Tapped resonator filter . . . . .	20
	c. Inductive resonator loading . . . . .	21
	C. Implementation . . . . .	25
	1. Fabrication and measurement . . . . .	25
	2. Quality factor . . . . .	28
III	DEVELOPMENT OF THE RF MEMS SWITCH MODEL . . . . .	31
	A. Introduction . . . . .	31
	B. Enhanced Modeling of RF MEMS Series Metal-contact Switch . . . . .	32
IV	AN INDUCTIVELY-LOADED RF MEMS TUNABLE FILTER WITH ADJUSTABLE SPURIOUS SUPPRESSION . . . . .	40
	A. Introduction . . . . .	40
	B. Circuit Analysis and Design . . . . .	42
	1. Resonator design . . . . .	42
	2. Adjustable spurious suppression . . . . .	43
	3. Filter design . . . . .	44
	C. Fabrication and Measurement . . . . .	47

CHAPTER	Page
D. Fundamental Limitations in Filter Tuning . . . . .	50
V CONCLUSION AND FUTURE WORK . . . . .	52
A. Conclusion . . . . .	52
B. Future Work . . . . .	54
1. Multi-bit tunable filter . . . . .	54
2. Millimeter-wave RF MEMS tunable filter . . . . .	55
REFERENCES . . . . .	57
VITA . . . . .	62



## LIST OF TABLES

TABLE		Page
I	Bandpass filter specifications . . . . .	8
II	Tunable Filter Model Element Values ( $Y_1 = Y_1' = 1/30$ S, $Y_2 = 1/100$ S, $Y_2' = 1/75$ S) . . . . .	46

## LIST OF FIGURES

FIGURE	Page
1	(a) Low pass prototype network for all-pole filter, and (b) low pass prototype network using inverters. . . . . 6
2	(a) General configuration of end-coupled microstrip bandpass filter, (b) equivalent bandpass prototype filter with J-inverters, and (c) equivalent circuit of a capacitive J-inverter. . . . . 8
3	Simulated $S_{21}$ for different values of $C_{12}$ . Higher frequency peak and lower frequency peak represent $f_m$ and $f_e$ respectively. . . . . 11
4	Variation of coupling coefficient with coupling capacitance. . . . . 12
5	Equivalent circuit of a singly loaded resonator. . . . . 13
6	Variation of external quality factor with input/output coupling capacitance. . . . . 14
7	Layout of the end-coupled filter. All dimensions are in mm. . . . . 15
8	Simulated performance of end-coupled filter. . . . . 15
9	(a) Stepped-impedance inductively loaded resonator, and (b) equivalent circuit for inductively loaded resonator. . . . . 16
10	Change in resonator center frequency expressed as a percentage tuning from unloaded resonator frequency as the line width ratio and length of inductive section is varied. . . . . 17
11	(a) Proposed layout of inductively loaded end coupled filter, and (b) simulated performance of inductively loaded end-coupled filter. . . . . 19
12	(a) Variation of mixed coupling coefficient with inter-resonator gap, and (b) variation of external quality factor with input/output coupling capacitance. . . . . 22

FIGURE	Page
13	(a) Proposed layout of the tapped resonator filter which provides suppression of the higher spurious passband. All dimensions are in mm. (b) Simulated filter performance. . . . . 23
14	(a) Layout of the inductively loaded tapped resonator filter, and (b) simulated performance of the inductively loaded tapped resonator filter. . . . . 24
15	(a) Fabricated end coupled filter without inductive loading, and (b) simulated and measured results. . . . . 26
16	(a) Fabricated end coupled filter with inductive loading, and (b) simulated and measured results. . . . . 26
17	(a) Fabricated tapped resonator filter without inductive loading, and (b) simulated and measured results. . . . . 27
18	(a) Fabricated tapped resonator filter with inductive loading, and (b) simulated and measured results. . . . . 27
19	Detailed structure of the RF MEMS switch from Radant MEMS Inc. 33
20	(a) Photograph, (b) side view and (c) simple model of the Radant MEMS switch. . . . . 33
21	(a) Top view, (b) side view, and (c) enhanced model of a mounted RF MEMS switch on RT/Duroid substrate. . . . . 35
22	(a) Simulated s-parameter magnitude response, and (b) simulated phase response of the equivalent capacitance between the switch landing pad and the RT/Duroid substrate ground. . . . . 36
23	(a) Simulated s-parameter magnitude response, and (b) simulated phase response of the bond-wire model and series R-L circuit with $L_b = 0.8$ nH and $R_b = 0.1\Omega$ . . . . . 38
24	(a) Proposed resonator structure, and (b) equivalent circuit of the resonator with ideal switches in the up-state position ( $Y_2 < Y_1$ ). . . . 41
25	Equivalent circuit of the reconfigurable open-ended stub with ideal switches in the up-state position. . . . . 43

FIGURE	Page
26	(a) Proposed filter layout, and (b) equivalent half-circuit model of the filter in the up-state condition. . . . . 45
27	Circuit simulation of the tunable filter with adjustable harmonic suppression when all the switches are in the up-state position. . . . . 47
28	Photograph of the fabricated RF MEMS tunable filter. . . . . 48
29	(a) Simulated filter s-parameters with switches in up-state and down-state positions including the effect of enhanced switch model. (b) Measured filter performance for two different states. . . . . 49
30	Inductive loading section for multi-state tunable filter. . . . . 54
31	Millimeter-wave RF MEMS tunable filter for 24-31 GHz applications. 56
32	Simulated results of the 24-31 GHz RF MEMS tunable filter. . . . . 56

## CHAPTER I

### INTRODUCTION

#### A. Tunable Filter Applications

Electrical filters have the property of frequency-selective transmission which enables them to transmit energy in one or more passbands and to attenuate energy in one or more stopbands. Major advances and development in the field of microwave filters were mainly during World War II at M.I.T Radiation Laboratory, Harvard Radio Research Laboratory, etc and research was mostly devoted to the development of Electronic Counter Measures (ECM) for radar applications. ECM systems involve Electronic Support Measures (ESM) systems that classify incoming radar signals by amplitude, pulse-width, frequency, etc, to identify and intercept radio communication signals [1]. Appropriate counter-measures such as jamming could then be taken based on the identity of the intercepted signal. Frequency resolution of signals can be achieved by splitting the entire microwave range into smaller sub-bands and by using mechanically, magnetically or electronically tunable filters with fast-tuning speed to scan the whole receive band.

Microwave filters are essential components of Radio Frequency (RF) front-end communication systems for mobile and base station applications. The advent of multi-standard wireless handsets require frequency-agile RF front ends that support communication at multiple frequencies. Tunable filters are employed in transmitters and receivers of multi-band or frequency-hopped transceivers.

---

The journal model is *IEEE Transactions on Microwave Theory and Techniques*.

## B. Filter Tuning Techniques

The tuning mechanism in tunable filters can be classified into three major types: mechanical, magnetic and electronic [2].

Mechanically tunable bandpass filters are realized using co-axial or waveguide resonators and have large power-handling capability and low insertion loss. These manually tuned filters have slow tuning speed and are often large and bulky for application in modern integrated systems [3].

Magnetically tunable bandpass filters have been used extensively in microwave communication systems and have single-crystal Yttrium-Iron-Garnet (YIG) spheres in their resonators that are tuned by changing the biasing current (typically hundreds of milliamperes). Advantages of such filters are multi-octave tuning range, spurious free response, low insertion loss and high quality factor (Q-factor), while their disadvantages are size, power consumption, tuning speed and incompatibility in integrated systems [4], [5].

Electronically tunable filters typically employ variable capacitors that are controlled by applying a bias voltage, thereby tuning the resonator. These filters provide octave tuning range, compact size, fast tuning and compatibility to integrated front ends. Several technologies are used to provide variable capacitors in tunable filters such as semiconductor diodes (gallium arsenide, silicon and silicon germanium), ferroelectric thin-films and RF microelectromechanical (MEMS) switches. Among these technologies, semiconductor diodes suffer from poor power handling, non-linear behavior and low Q-factor at microwave frequencies [6], [7]. Barium Strontium Titanate (BST) ferroelectric thin films provide high tunability at room temperature and have a relatively high power handling capability. They are easily implemented in integrated planar structures and enable compact designs but suffer from poor linearity hence

limiting the dynamic range of systems [8].

Recently, RF MEMS technology has provided means of creating highly linear, low-loss electromechanical switches that either provide an open circuit with a small capacitance (10-80 fF) or a short circuit with a small resistance (0.6-1  $\Omega$ ). MIT Lincoln Laboratory [9], Raytheon [10] and Radant MEMS Inc. [11] have developed miniature switches with moving metal membranes in series or shunt configuration, that are actuated by an applied voltage bias. RF MEMS switches have several distinct advantages such as very low insertion loss (0.05-0.2 dB), very high linearity ( $IIP_3 > 60$  dBm), extremely low power consumption due to electrostatic actuation and very high isolation. They are very suitable for highly integrated systems and have been widely used in miniature switchable filters, phase shifters, etc [12]. The disadvantages of RF MEMS are low power handling capability (<1-2W), medium switching speed (3-100  $\mu s$ ), reliability and requirement for hermetic packaging. Ongoing research in RF MEMS concentrate on improving these drawbacks and efforts are being made to make RF MEMS compatible with integrated circuit foundry processes.

### C. Thesis Overview

This thesis comprises of the theory and design of novel fixed and RF MEMS-based tunable microstrip filters for microwave applications. Chapter II deals with the design of a fixed end-coupled microstrip filter with inductive loading. This filter is then extended to design a novel inductively loaded microstrip filter with tapped input-output coupling and mixed inter-resonator coupling. These fixed filters are fabricated and measurement results are provided. Chapter III deals with RF MEMS switch technology and the switch parameters for the packaged series metal-contact RF MEMS

switch from Radant MEMS Inc.<sup>1</sup>, which is used in the design of the tunable filter. Chapter IV describes the design of a tunable RF MEMS filter based on the topologies investigated in Chapter II. The upper rejection skirt of the filter is improved by developing means of simultaneously suppressing the spurious harmonic resonance as the filter is tuned. The fabricated filter and measured performance are presented. Chapter V is the conclusion and future work.

---

<sup>1</sup>Radant MEMS Inc., Stow, MA



## CHAPTER II

DESIGN OF INDUCTIVELY-LOADED FIXED-TUNED  
MICROSTRIP FILTERS

## A. Introduction

RF bandpass filters are essential components in RF heterodyne receivers where they act as image reject filters before the first down-converter to prevent the image frequency from appearing in the intermediate frequency (IF) band. In heterodyne architectures, they are also used as channel select filters to minimize out-of-band interference. Microstrip technology is popular in mobile wireless applications due to its light weight, compactness and relatively low-loss. Various planar microstrip bandpass filter topologies have been developed based on butterworth, chebyshev and elliptic function responses to provide the required rejection performance in receiver systems [13].

The design of microwave filters is normally accomplished by using a two-port lumped element network called a lowpass prototype with an angular cutoff frequency of 1 rad/s and reference impedance of  $1\Omega$ . Network synthesis [14] enables the design of these prototype networks to meet an approximating transfer function such as chebyshev, elliptic function, etc. Fig. 1(a) shows the ladder lowpass prototype network for an all-pole (transmission zeros at infinity) network and Fig. 1(b) shows the lowpass filter implementation with admittance inverters and shunt capacitors. The dual implementation of these networks using impedance inverters and series inductors is possible. The optimally selective function for an all-pole prototype is the chebyshev filter with equi-ripple response in the passband and monotonically increasing rejection in the stopband. The order of the chebyshev lowpass network for a given rejection performance can be determined by equations given in [13]. The designed

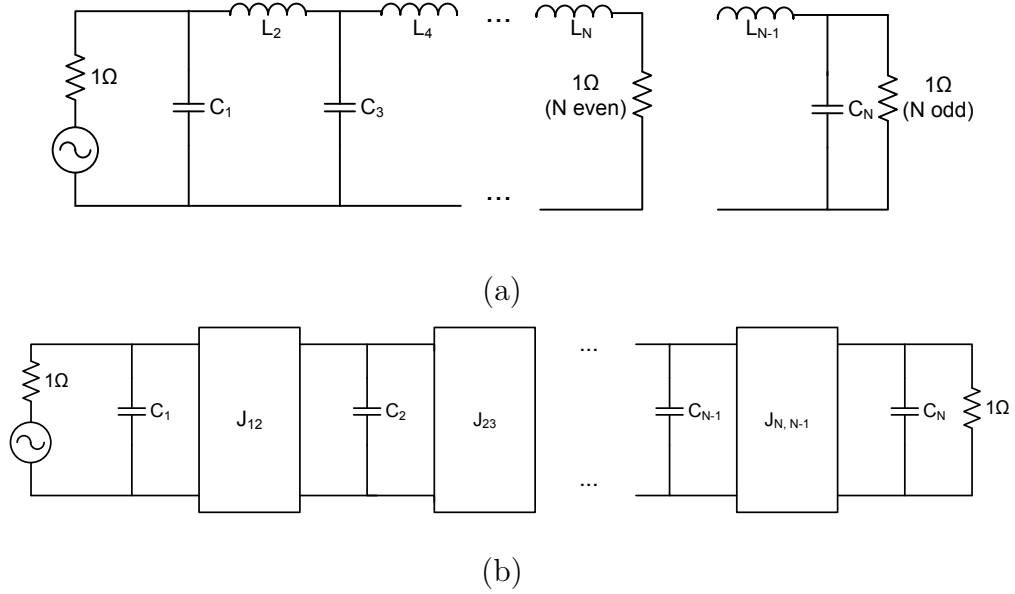


Fig. 1. (a) Low pass prototype network for all-pole filter, and (b) low pass prototype network using inverters.

lowpass prototype network is then converted to its bandpass equivalent by the use of transformation equations [13]. The filter structures developed in this chapter can be generally classified as coupled resonator filters and the underlying principles involving the design of such structures has been well established by Cohn [15],[16]. Filter design is based on the use of quarter or half-wavelength microstrip resonators as series and shunt resonators respectively and inductively or capacitively coupled microstrip lines as impedance or admittance inverters. The design, simulation and fabrication of capacitively coupled filters with inductively loaded resonators and tapped resonator coupling for spurious resonance suppression is presented in this chapter.

## B. Design

This section describes the design of two fixed filters: Traditional end-coupled filter and mixed coupled filter with tapped resonators. A slow-wave resonator is created

by inductively loading the resonator with a step in resonator impedance and the corresponding shift in resonant frequency is studied. The filter design methodology for both filters is presented.

The general configuration of an open-ended half-wavelength resonator two-pole microstrip filter and its equivalent circuit are shown in Fig. 2(a), 2(b). The half-wavelength resonators have a physical length ' $l$ ' and characteristic admittance  $Y_0$ , and act as shunt LC resonators. The microstrip gaps provide a coupling capacitance ( $C_{i,i+1}, i = 0, 1, 2$ ) due to fringing electric fields at the ends of the resonators. The reactance associated with a capacitance  $C_{i,i+1}$  is represented by  $B_{i,i+1}$ . The equivalent  $\pi$ -model representation of the series gap capacitance is used to realize a J-inverter in the filter structure, as shown in Fig. 2(c). The electrical length of the microstrip resonator is reduced to adjust for the negative shunt capacitances provided by the J-inverters. The input and output ports are microstrip lines with  $Y_A=50 \Omega$  and is typically achieved with a tapered microstrip transition for  $Y_A \neq Y_0$ .

The design of end-coupled microstrip resonator filters can be accomplished with the use of design equations in [13] but a more general computer-aided design methodology introduced by Dishal [17],[18] is employed for the design of filters in the rest of this thesis. The design specifications for the end-coupled microstrip filter are shown in Table. I. The low-pass prototype element values for the given specifications are:  $g_0 = 1, g_1 = 0.6323, g_2 = 0.5269, g_3 = 1.1999$ . The given passband ripple value (0.036 dB) ensures that there is at least 20.8 dB (1.2 VSWR) return loss at the filter input and output.

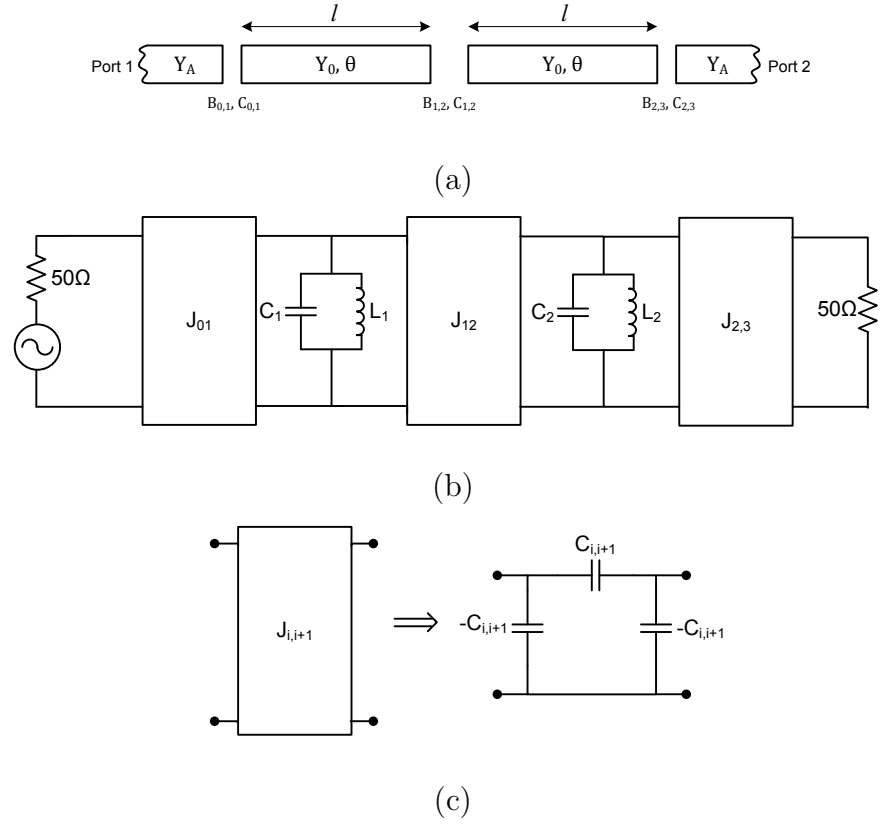


Fig. 2. (a) General configuration of end-coupled microstrip bandpass filter, (b) equivalent bandpass prototype filter with J-inverters, and (c) equivalent circuit of a capacitive J-inverter.

Table I. Bandpass filter specifications

Center Frequency	1.5 GHz
Fractional Bandwidth (FBW)	5%
Filter response	All pole Chebyshev
Number of poles	2
Passband ripple	0.036 dB

## 1. End-coupled microstrip filter

### a. Methodology

Any narrow-band, lumped element or distributed bandpass filter can be completely described by three fundamental quantities: synchronous tuning frequency,  $f_0$ , coupling between adjacent resonators,  $K_{i,i+1}$ , and the singly loaded external quality factor,  $Q_{ext}$ , of the input and output resonators. From the given specifications, the inter-resonator coupling,  $K_{i,i+1}$ , and external quality factor,  $Q_{ext}$ , can be derived for the general case of an N-pole filter as [14]:

$$K_{i,i+1} = \frac{FBW}{\sqrt{g_i \cdot g_{i+1}}} \quad (2.1)$$

$$Q_{ext_1} = \frac{g_0 \cdot g_1}{FBW} \quad (2.2)$$

$$Q_{ext_N} = \frac{g_N \cdot g_{N+1}}{FBW} \quad (2.3)$$

where  $i = 1, \dots, N - 1$ , FBW is the fractional filter bandwidth and  $g_0, \dots, g_{N+1}$  are the lowpass prototype values for a chebyshev filter of order N with given ripple in the passband.

Eqns. (2.1), (2.2) and (2.3) are evaluated for the prescribed specifications resulting in  $Q_{ext_1} = Q_{ext_2} = 12.64$  and  $K_{12} = 0.08665$ . The design of the filter involves converting the calculated values of  $Q_{ext}$  and  $K_{12}$  into equivalent physical parameters involving open-ended half-wavelength microstrip resonators.

The microstrip filter is designed on RT/Duroid 6010LM with permittivity of  $\epsilon_r = 10.2$  and thickness of 2.54 mm. The characteristic impedance of the resonator is chosen to be  $Y_0 = 30 \Omega$  which corresponds to a line width of 5.5 mm. The effective permittivity of the substrate at 1.5 GHz is found to be  $e_{ref} = 7.6$  from full-wave sim-

ulations using a commercial EM simulator, SONNET<sup>1</sup>, assuming that the substrate material is non-dispersive in nature. The length of the half-wavelength microstrip resonator is calculated as  $l = 33$  mm.

The end-coupled filter structure has purely electric coupling due to fringing electric fields at the open ends of the resonators and hence the inter-resonator electric coupling coefficient is found as a function of inter-resonator capacitance ( $C_{12}$ ) [19]. The coupling coefficient between two resonators can be completely characterized by the electric resonance frequency ( $f_e$ ) and magnetic resonance frequency ( $f_m$ ) associated with the coupling mechanism. Since  $f_e$  and  $f_m$  are less and greater than resonator center frequency respectively for electric coupling, the resonator is detuned by loose input/output coupling ( $|S_{21}| \approx -30$  dB to  $-40$  dB, at resonator frequency) so that  $f_e$  and  $f_m$  can be identified for calculation of the coupling coefficient by full-wave EM simulation for different values of  $C_{12}$ . Fig. 3 shows the simulated  $S_{21}$  parameters for different values of  $C_{12}$ . The higher resonant peak corresponds to the magnetic resonant frequency ( $f_m$ ) and the lower resonant peak corresponds to the electric resonant frequency ( $f_e$ ). The coupling coefficient is calculated from,

$$K = \frac{f_m^2 - f_e^2}{f_m^2 + f_e^2} \quad (2.4)$$

The obtained K values are used as data points for a  $2^{nd}$  order polynomial curve fit as shown in Fig. 4. The polynomial equation is used as a reasonably accurate initial approximation to find the inter-resonator capacitance for a given coupling coefficient. It is observed that the resonator center frequency changes as the capacitance is varied. A correction for the shift in resonance frequency is adjusted in the resonator length, and the coupling coefficient is recalculated. Subsequent optimization results in accu-

---

<sup>1</sup>SONNET Software Inc. v11.52, Syracuse, NY

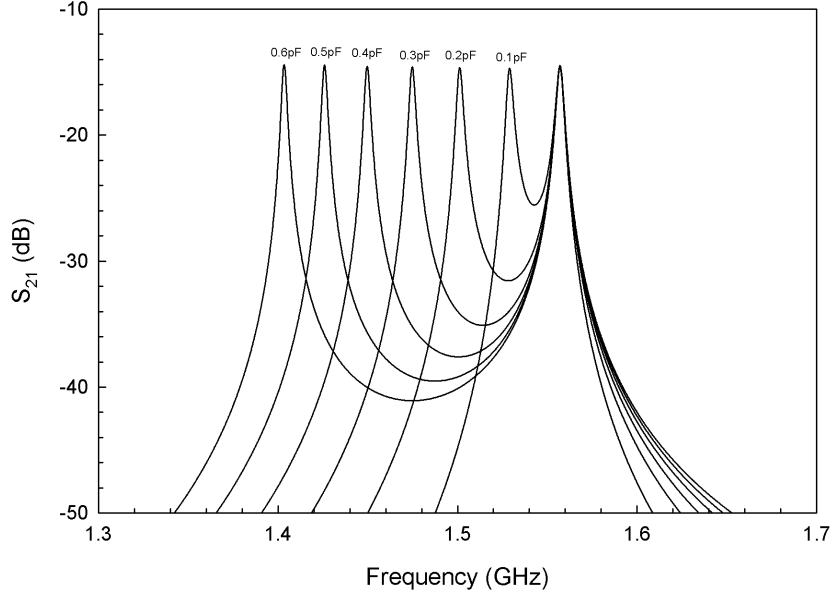


Fig. 3. Simulated  $S_{21}$  for different values of  $C_{12}$ . Higher frequency peak and lower frequency peak represent  $f_m$  and  $f_e$  respectively.

rate values for resonator length and capacitance. The required coupling coefficient ( $K_{12}=0.0866$ ) is achieved when the inter-resonator capacitance is  $C_{12} = 0.494$  pF. Once the required value of  $C_{12}$  is determined, it is realized in microstrip technology by a gap or inter-digital capacitor.

The phase response of a singly loaded resonator as shown in Fig. 5 is used to extract the external quality factor of the end resonators [13]. The phase response of  $S_{11}$  of the singly loaded resonator is found at the reference place  $T - T'$  with external conductance  $G$  attached to the lossless shunt LC resonator. Ideally, the absolute phase of  $S_{11}$  is zero at the resonant frequency and the external quality factor is found from,

$$Q_{ext} = \frac{f_0}{\Delta f_{\pm 90^\circ}} \quad (2.5)$$

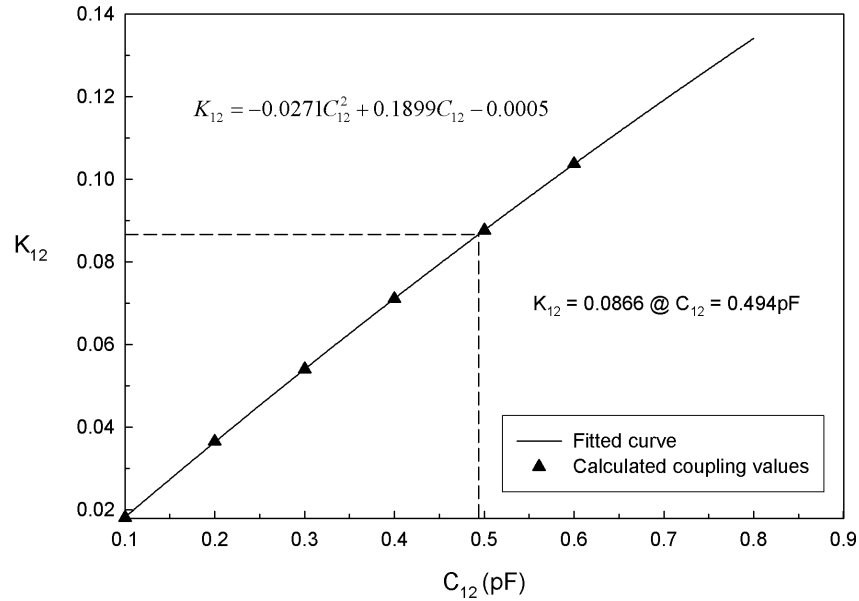


Fig. 4. Variation of coupling coefficient with coupling capacitance.

where  $f_0$  is the resonance frequency of the resonator and  $\Delta f_{\pm 90^\circ} = f_{+90^\circ} - f_{-90^\circ}$  is the frequency difference between points of absolute phase  $+90^\circ$  and  $-90^\circ$  respectively.  $Q_{ext}$  is extracted from full-wave EM simulation for different values of input/output coupling capacitance ( $C_{io}$ ) and a  $2^{nd}$  order polynomial curve is fit to the calculated data points. The reference plane  $T-T'$  in Fig. 5 may not be located at the same point in EM simulation thus resulting in non-zero absolute phase at resonant frequency. A correction is enforced to account for this phenomenon by calculating  $\pm 90^\circ$  offsets from the non-zero absolute phase value at resonant frequency. Fig. 6 shows the variation of external quality factor with input/output coupling capacitance and shows that  $C_{io} = 1.83$  pF is necessary to achieve the calculated external quality factor,  $Q_{ext} = 12.64$ .

Fig. 7 shows the designed layout of the end coupled microstrip filter. The inter resonator capacitance  $C_{12}$  is implemented as an four finger interdigital capacitor



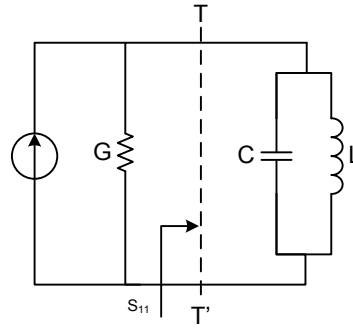


Fig. 5. Equivalent circuit of a singly loaded resonator.

with dimensions as shown in Fig. 7 while the external coupling capacitors  $C_{io}$  are implemented as lumped surface-mount capacitors due to their large capacitance value. Fig. 8 shows the full-wave EM simulation of the filter structure with dielectric loss included. A shift in filter center frequency is observed due to existence of shunt parasitic capacitances in the interdigital capacitor. These contribute to an excess phase length which shifts the bandpass response to lower frequencies. Correction in resonator length must be incorporated to ensure that the bandpass response is centered around the designed frequency of 1.5 GHz.

The simulated response of the end-coupled microstrip filter shows the presence of a second spurious response due to the resonance between capacitive inverters and inductive open-ended resonators as they are tuned to lower frequencies [20]. Only dielectric loss is considered in the simulation and is observed to be around 0.5 dB. For the rest of the filters designed and fabricated in this thesis, the dielectric loss remains almost the same. Any additional loss arises due to radiative losses and losses due to external components such as capacitors, connectors and switches. The presence of a spurious response degrades the rejection in the upper skirt of the filter response and hence it is not desirable. Methods will be developed later in this thesis which result in the suppression of the spurious response to improve the upper rejection skirt

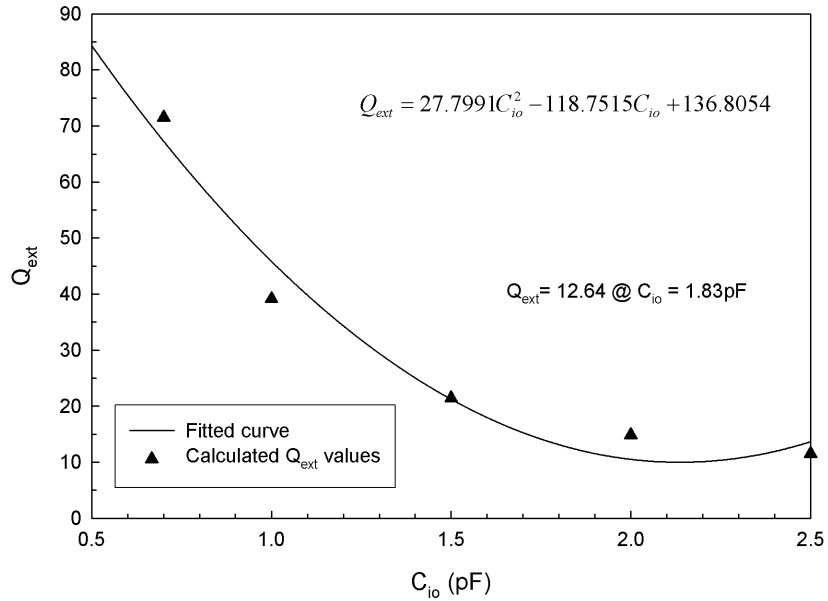


Fig. 6. Variation of external quality factor with input/output coupling capacitance of the filter.

#### b. Inductive resonator loading

Inductively or capacitively loaded resonators are used in miniature filter design to create “slow-wave” resonators through which signals propagate with a phase velocity lesser than the natural phase velocity that is determined by the guided wavelength in the medium [21]. By decreasing the phase velocity through a resonator, the resonator appears electrically longer and resonates at a lower frequency. Recently, the loading technique has been extended to the design of tunable filters by switching inductive or capacitive loading elements to provide controllable phase velocity in the resonator [22]. The loading mechanism in [21] and [22] is based on capacitive resonator loading with shunt capacitive RF MEMS switches in short-ended CPW resonators at the point of maximum voltage. The dual of this topology, i.e., series inductive loading

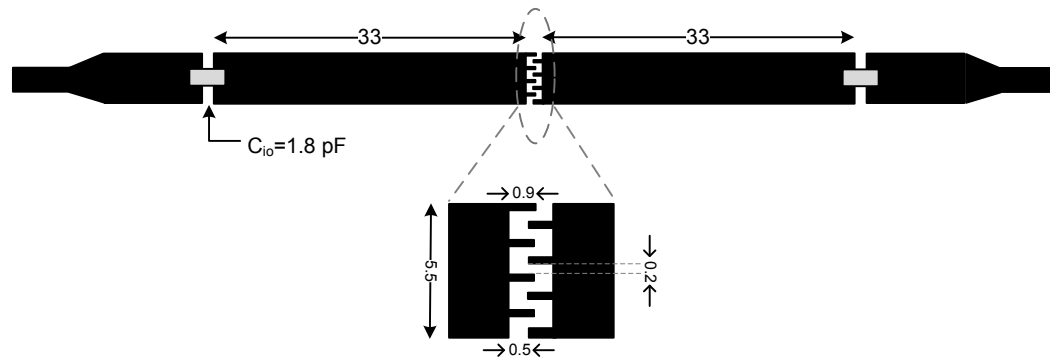


Fig. 7. Layout of the end-coupled filter. All dimensions are in mm.

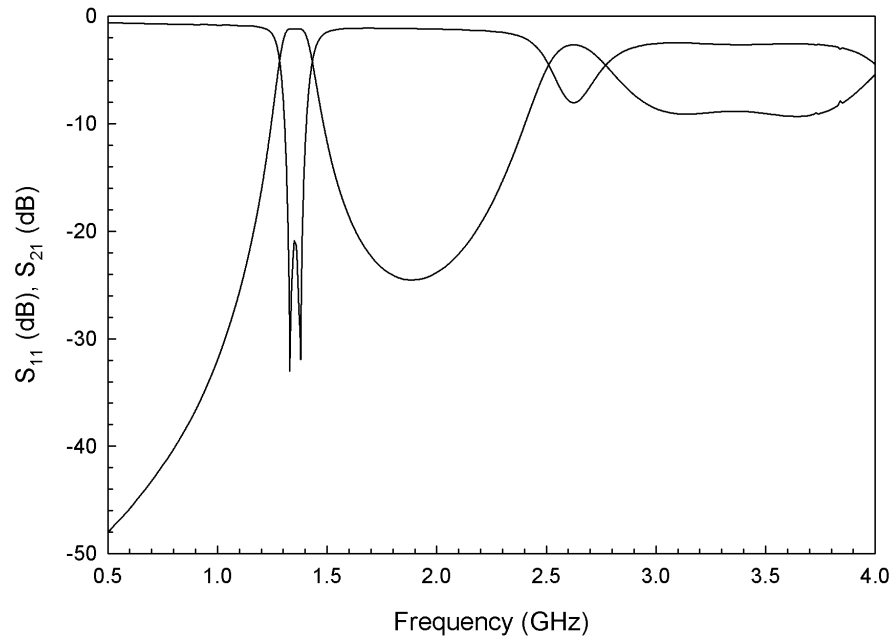


Fig. 8. Simulated performance of end-coupled filter.

in microstrip resonators at the point of maximum current density is discussed in the following paragraphs.

Consider the inductively loaded resonator and the equivalent circuit of the loading section shown in Fig. 9(a) and 9(b). A microstrip stepped impedance discontinuity is equivalent to a series inductance with parasitic shunt capacitances at the step interface [13]. The parameter  $r$  is considered to be the ratio of widths  $w_1$  to  $w_2$  ( $0 < r \leq 1$ ) and the length of loading section  $l_s$  is located at a distance  $d_s$  from one of the open ends of the microstrip resonator.

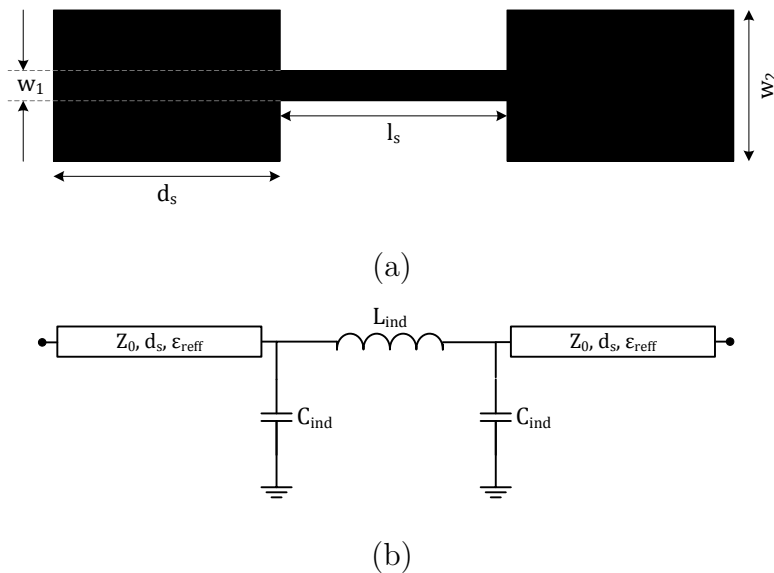


Fig. 9. (a) Stepped-impedance inductively loaded resonator, and (b) equivalent circuit for inductively loaded resonator.

The values of  $r$ ,  $d_s$  and  $l_s$  determine the shift in the resonant frequency of the stepped-impedance resonator, and hence the effect of these parameters on the resonator will be studied. Analytical expressions for the stepped-impedance resonator will be developed in chapter IV. It is of interest here to establish a parametric study of the shift in resonance as the constitutive parameters are varied. Fig. 10 shows the variation of resonance frequency as  $r$  and  $l_s$  are varied with the inductive discontinuity

placed in the middle of the resonator.

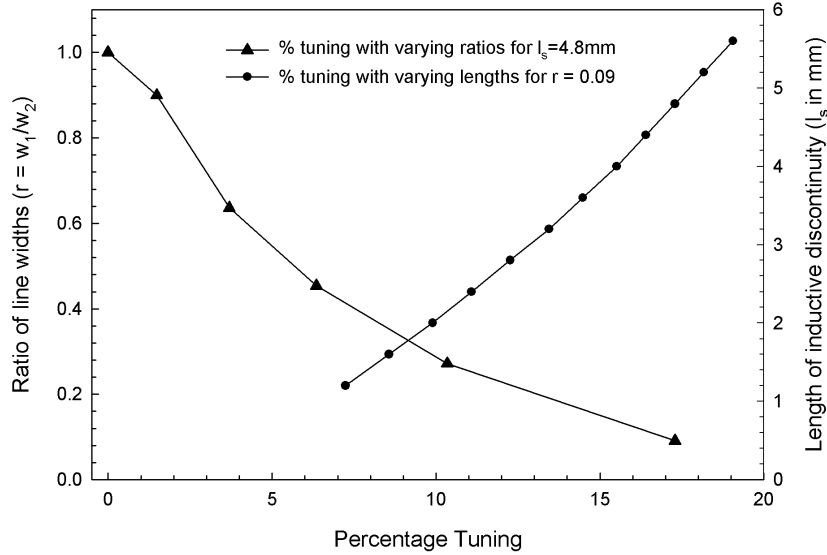


Fig. 10. Change in resonator center frequency expressed as a percentage tuning from unloaded resonator frequency as the line width ratio and length of inductive section is varied.

It is seen that smaller values of  $r$  provide greater shift in resonance frequency. The smallest value of  $r$  is restricted by manufacturing tolerances and should be considered in design. Empirical formulas for the determination of equivalent circuit parameters  $L_{ind}$  and  $C_{ind}$  in the microstrip discontinuities is found in [13]. Parasitic shunt capacitance  $C_{ind}$  provides partial capacitive loading in the resonator apart from inductive loading by  $L_{ind}$  and causes the resonance to shift to still lower frequencies. Increasing  $l_s$  causes  $L_{ind}$  to have higher values thus causing greater loading effect on the resonator. The highest shift in resonance frequency for a given  $r$  and  $l_s$  occurs when the loading section is located in the middle of the resonator, i.e., at the point of highest current density. Based on these design curves, an inductively loaded microstrip filter is designed with  $r = 0.0909$  and  $l_s = 4.8$  mm with the loading section located in the

middle of the resonator. Fig. 11(a) shows the proposed layout of the filter and Fig. 11(b) shows the obtained full-wave simulation considering the effect of dielectric loss mechanisms.

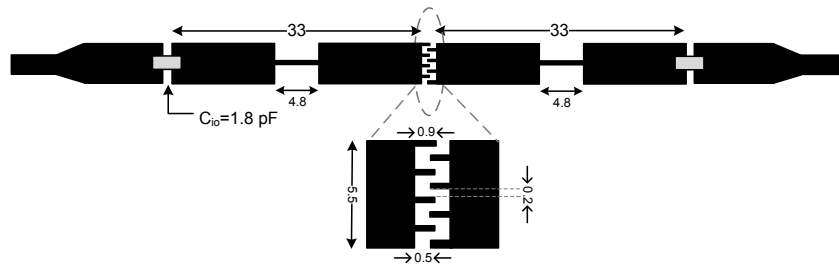
The inductively loaded end-coupled filter also shows a higher spurious passband response that degrades the upper rejection skirt of the filter. Tamijani et al. have shown that the spurious passband can be moved to higher frequencies ( $> 3f_0$ ) by using distributed loading techniques [21]. Since the proposed inductive loading mechanism is lumped in nature, alternate solutions are required to ensure suppression of the spurious band.

## 2. Tapped resonator microstrip filter with mixed coupling

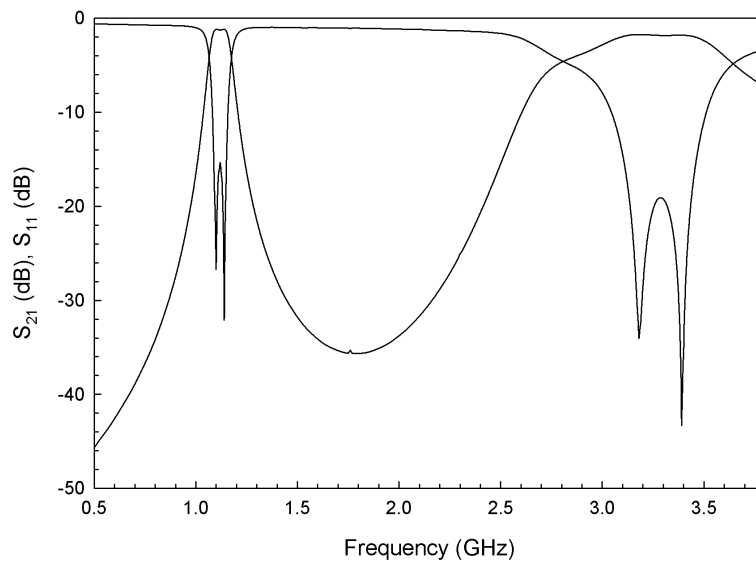
### a. Suppression of spurious responses

As discussed in the previous section, the decreased upper skirt due to spurious passband response can result in filter performance that is unacceptable in many systems due to insufficient adjacent channel rejection. Several methods have been developed to suppress the spurious responses of microstrip filters by equalizing the even and odd mode phase velocities of the wave traveling through the microstrip filter. In [23], over-coupled end stages of the filter with increased image impedance is used to equalize phase velocities in high  $\epsilon_r$  substrates. Apertures in the ground plane designed by quasi-TEM optimization routines are also used to suppress the second spurious passband by equalizing the even and odd mode phase velocity [24]. Meandered parallel coupled lines have been used to design miniature filters with spurious suppression at the second harmonic frequency for wide bandwidth filters fabricated on high  $\epsilon_r$  substrates [25].

While these techniques depend on phase velocity equalization, the method dis-



(a)



(b)

Fig. 11. (a) Proposed layout of inductively loaded end coupled filter, and (b) simulated performance of inductively loaded end-coupled filter.

cussed in this section is based on a tapped microstrip filter that is used to provide a transmission zero at the spurious passband frequency to suppress it and hence improve the upper rejection skirt of the filter. The design of tapped resonator filters has been discussed in detail in [26]. The position of tapping on the resonator is based on the required spurious suppression frequency as well as the value of  $Q_{ext}$  that has to be satisfied.

#### b. Tapped resonator filter

The proposed tapped resonator microstrip filter is shown in Fig. 13(a) where  $t_s = 7.5$  mm is the position of the tap point from the open end of the resonator. A transmission zero at  $2f_0$  is introduced in the filter response by designing a filter with tapped resonators where the tapping distance  $t_s$  is a quarter wavelength long at  $2f_0$ , or equivalently, one-eighth wavelength at  $f_0$ . A quarter wavelength transformer at  $2f_0$  transforms the open end of the resonator to a short circuit at the tap point thereby suppressing the spurious passband. An approximate tap point is calculated based on  $\epsilon_{reff}$  of the substrate and the tapped resonator is simulated using an EM simulator.  $t_s$  is adjusted to get a voltage minimum at the tap point at  $2f_0$ . The value of  $Q_{ext}$  will be obtained by coupling the input/output lines with an appropriate coupling capacitance to the resonators.

An end-coupled microstrip filter designed with the tapped resonator will have purely electric inter-resonator coupling as discussed in the case of the end-coupled microstrip filter. Filter miniaturization can be achieved by using mixed inter-resonator coupling due to reduction in the overall area associated with the filter. Mixed coupling is characterized as the sum of electric and magnetic coupling coefficients [13]. By coupling the two resonators at any arbitrary point on the resonator, electric coupling is caused by fringing electric fields between the resonators and magnetic coupling is



caused by mutual inductance between currents flowing in each resonator. Fig. 13(a) shows the two resonators coupled at an arbitrary point and separated by an appropriate gap which determines the inter-resonator coupling co-efficient. The microstrip resonator with tapped input/output coupling and mixed inter-resonator coupling will have to satisfy the design requirements for  $Q_{ext}$  and  $k_{12}$  as derived in Section B.1.a for the filter design specifications in Table I.

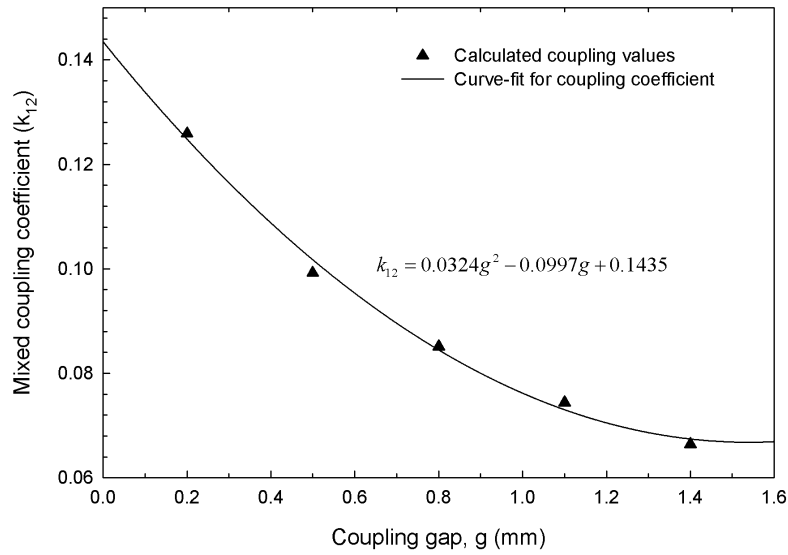
The filter is designed on RT/Duroid 6010LM with  $\epsilon_r = 10.2$ , and thickness of 2.54 mm. Dishal's method is used to extract the  $Q_{ext}$  and  $k_{12}$  design curves for the filter. The variation of  $Q_{ext}$  with input/output coupling capacitance and the variation of  $k_{12}$  with inter-resonator gap is shown in Fig. 12(a) and Fig. 12(b) respectively.

The required value of  $Q_{ext}$  is achieved when the input/output coupling capacitance is 2.2 pF and  $k_{12}$  is achieved when the inter-resonator gap is 0.8 mm.

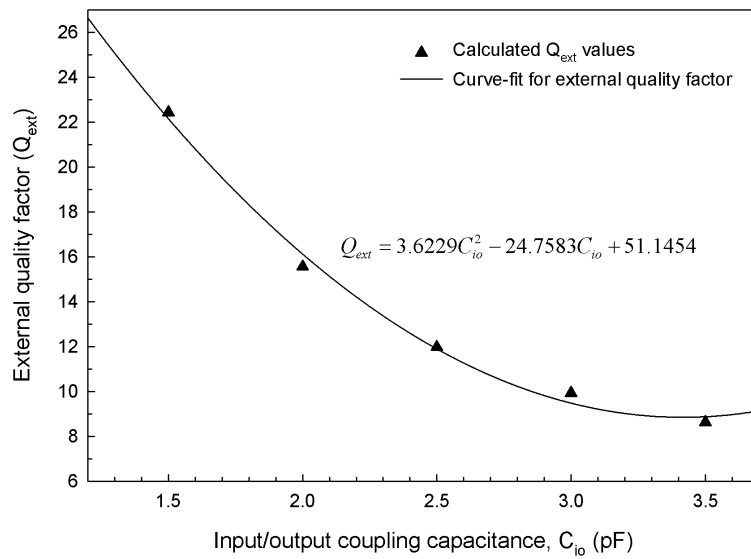
Fig. 13(b) shows the simulated performance of the tapped microstrip filter with the only loss mechanism being the dielectric loss tangent of the substrate. The center frequency of the filter is  $f_0 = 1.45$  GHz and the suppressed frequency harmonic at  $2f_0 = 2.9$  GHz is suppressed to  $> 40$  dB. This improves the upper rejection skirt of the filter compared to the equivalent end-coupled microstrip filter performance in Fig. 8.

### c. Inductive resonator loading

The inductive loading mechanism described in Section. B.1.b can be used to change the resonant frequency of the tapped resonator filter. An inductive discontinuity with  $r = 0.0909$  and  $l_s = 4.8$  mm placed in the middle of the resonator is used to create a loaded tapped-resonator filter. The layout of the filter is shown in Fig. 14(a) where all the dimensions remain the same as the unloaded tapped-resonator filter except for the addition of the loaded section. With this implementation, the center

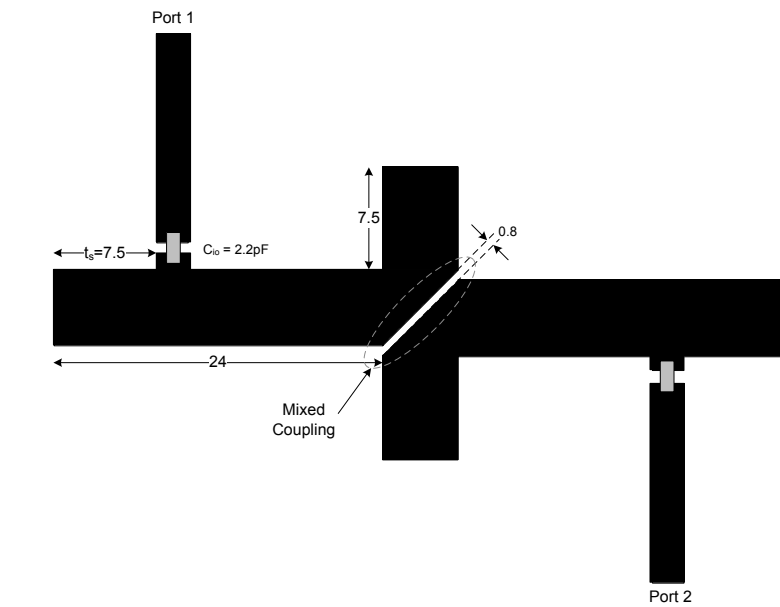


(a)

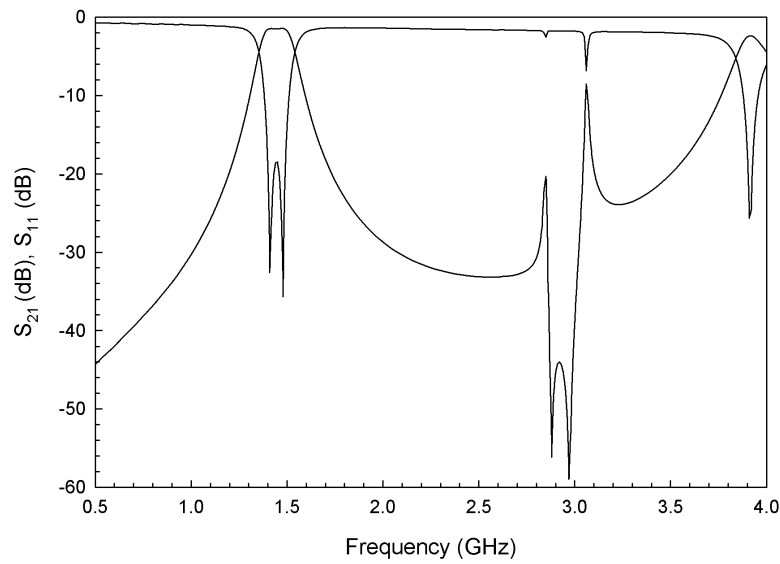


(b)

Fig. 12. (a) Variation of mixed coupling coefficient with inter-resonator gap, and (b) variation of external quality factor with input/output coupling capacitance.

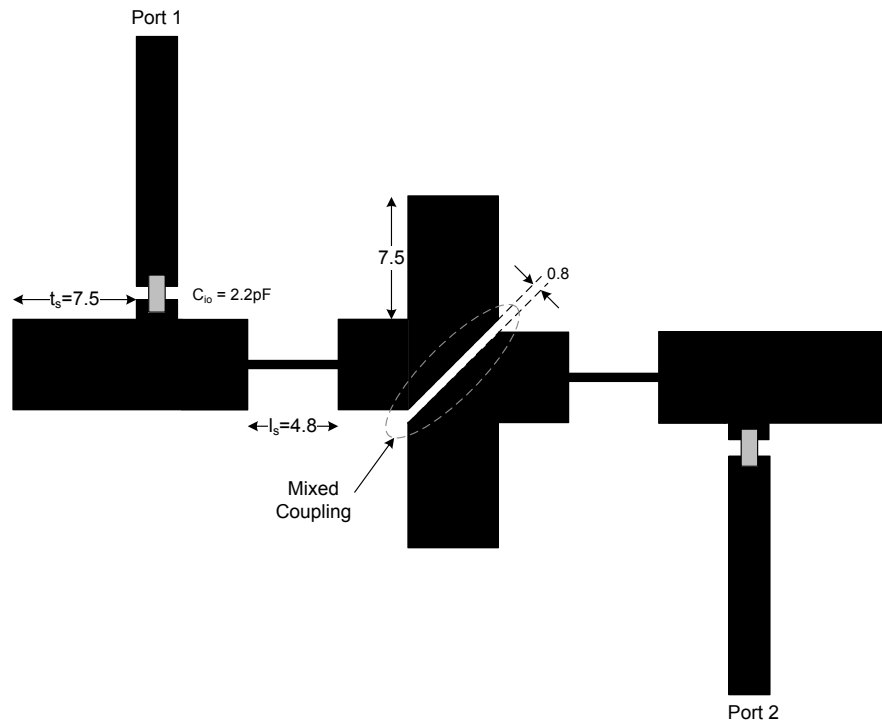


(a)

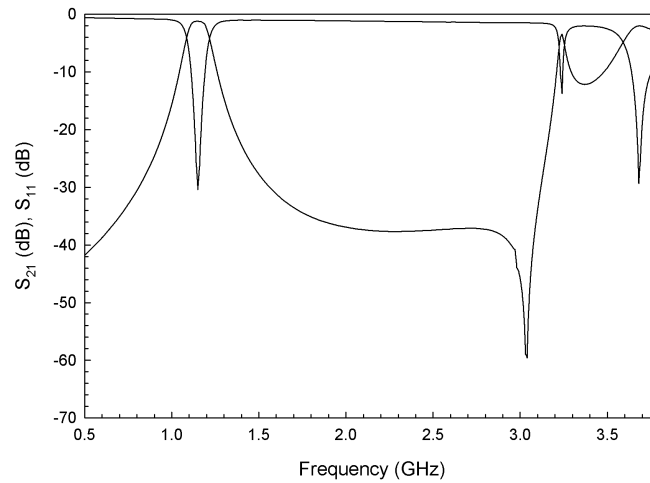


(b)

Fig. 13. (a) Proposed layout of the tapped resonator filter which provides suppression of the higher spurious passband. All dimensions are in mm. (b) Simulated filter performance.



(a)



(b)

Fig. 14. (a) Layout of the inductively loaded tapped resonator filter, and (b) simulated performance of the inductively loaded tapped resonator filter.

frequency of the filter is moved to a lower frequency but the transmission zero due the tapped resonator remains unaltered. This implies that as the filter center frequency is changed, its higher spurious suppression mechanism is unaltered thereby resulting in non-optimum upper rejection skirt performance. A mechanism to control the quarter wavelength stub at input and output of the filter will be introduced in chapter IV enabling the spurious suppression frequency to move as the filter performance is changed, thus maintaining a reasonably constant upper rejection skirt.

Fig. 14(b) shows the full-wave simulation of the filter performance. It is seen that the center frequency has changed from 1.45 GHz to 1.14 GHz due to inductive loading, resulting in 21.3% change in center frequency with respect to the unloaded filter center frequency.

## C. Implementation

### 1. Fabrication and measurement

The filters designed in the previous section are all fabricated on RT/duroid 6010LM high frequency substrate with a thickness of 2.54 mm and permittivity  $\epsilon = 10.2 \pm 0.25$ . The copper cladding is 1 oz. electrodeposited copper which corresponds to  $35\mu\text{m}$  thick copper foil. The filters are fabricated using a standard PCB etching process and SMA connectors are mounted on the input/output ports to facilitate the measurement. Standard full 2-port S parameter measurements are made on an Agilent 8719ES network analyzer by calibrating out the effect of cables and connectors using Load-Reflect-Match (LRM) technique.

Figs. 15, 16, 17 and 18 show the fabricated filters along with good agreement between simulated and measured results. The end-coupled filters have a center frequency shift from 1.36 GHz to 1.03 GHz in the unloaded and loaded cases respectively.

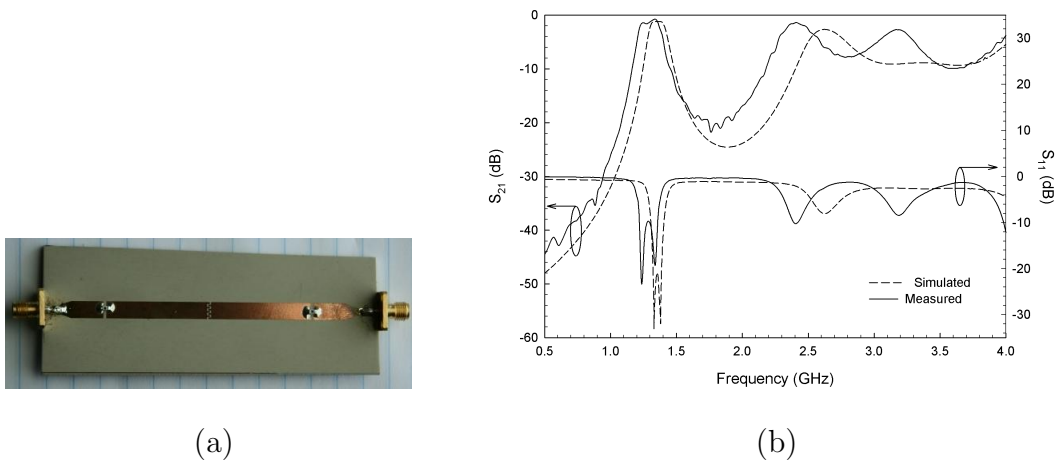


Fig. 15. (a) Fabricated end coupled filter without inductive loading, and (b) simulated and measured results.

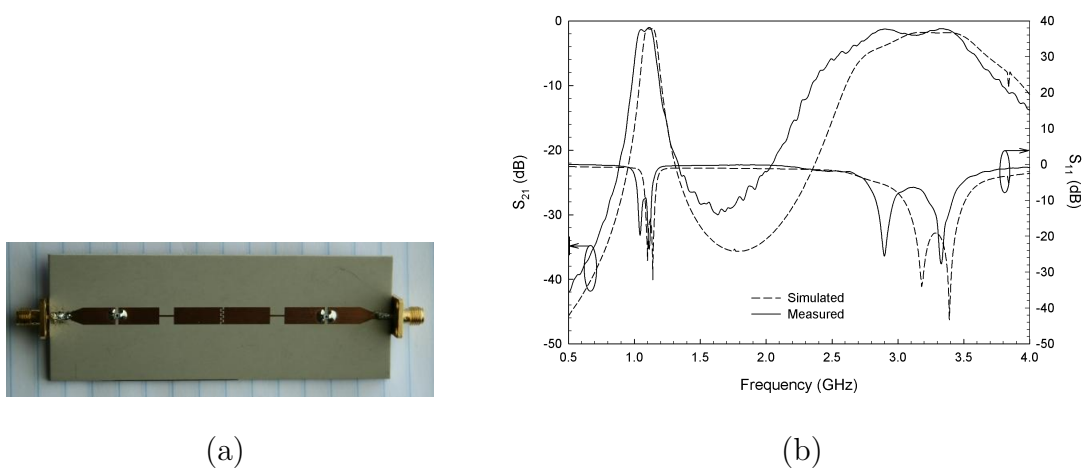


Fig. 16. (a) Fabricated end coupled filter with inductive loading, and (b) simulated and measured results.

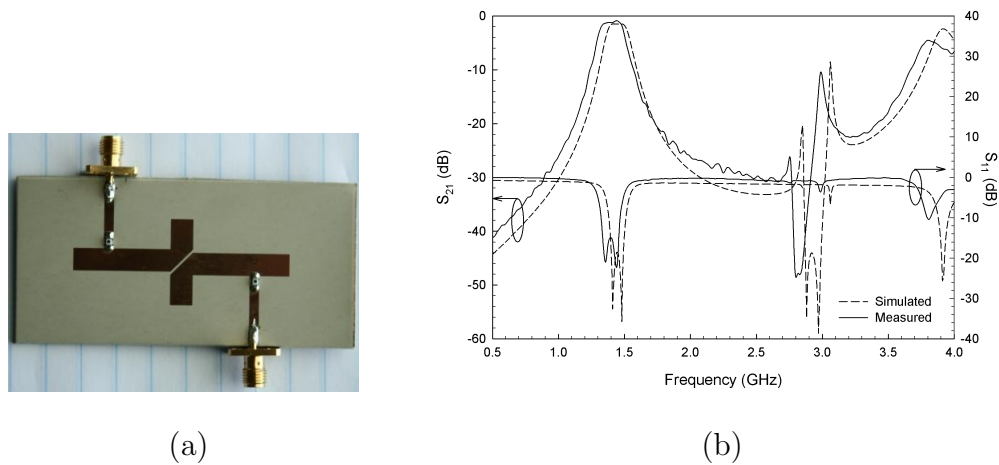


Fig. 17. (a) Fabricated tapped resonator filter without inductive loading, and (b) simulated and measured results.

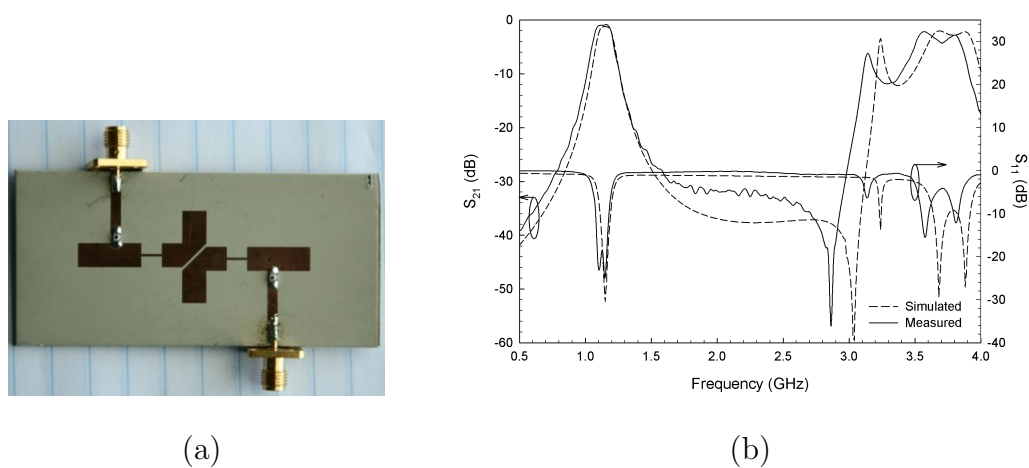


Fig. 18. (a) Fabricated tapped resonator filter with inductive loading, and (b) simulated and measured results.

The tapped-resonator filters have a center frequency shift from 1.40 GHz to 1.13 GHz in the unloaded and loaded cases respectively. The measured responses have show a frequency shift of 0.1-0.15 GHz from the simulated responses due to uncertainty in the exact value of the dielectric constant of the substrate. The insertion losses of the end-coupled and tapped resonator filters are 1.2 dB and 1.5 dB respectively. The effect of introducing a discontinuity in the resonator does not have a significant effect on the filter's insertion loss. However, there are a few discrepancies that need to be explained. In the case of the end coupled filters, the matching performance is better than -10 dB in the measurements while the designed return loss is better than -15 dB. This arises due to imperfect positioning of the input/output surface-mount capacitor along the width of the resonator because of smaller width of the capacitor compared to the width of the microstrip line thus decoupling the input/output from the filter. Since there is no uncertainty in the position of the surface-mount capacitor in the tapped resonator filter (the capacitor and microstrip line have similar widths), the measured return loss is better than 15 dB and closer to the designed value. The slight mismatch in high frequency performance ( $> 2$  GHz) is attributed to fabrication sensitivity at higher frequencies and the dispersive nature of the substrate which was not accounted for in design.

## 2. Quality factor

The quality factor of a resonator (Q) is a figure of merit that quantifies the energy dissipated by a resonant circuit. The general definition for the Q-factor is given by,

$$Q = \omega \frac{\text{energy stored in resonator}}{\text{power dissipated}} \quad (2.6)$$



At resonance, the Q-factor is,

$$Q = \omega_0 \frac{W_m + W_e}{P_{loss}} = \omega_0 \frac{2W_m}{P_{loss}} \quad (2.7)$$

where  $\omega_0$  is the resonant frequency,  $W_m$  and  $W_e$  are the average magnetic and electric energies stored in the resonant structure and  $P_{loss}$  is the power loss. At resonance, the electric and magnetic energies are equal.

In practice, for a resonator to be used in a system, it has to be loaded by external circuitry. The losses associated with the external circuitry adds to the losses in the resonant structure and affects the Q-factor measurement of the resonant structure. In order to measure the Q-factor of the resonant structure exactly, the Q-factor associated with the external circuitry ( $Q_{ext}$ ) has to be known. The Q-factor of the resonant structure and the external circuitry is called the loaded Q-factor ( $Q_L$ ) and is found by direct measurement. The Q-factor associated with the resonant structure alone is called the unloaded Q-factor ( $Q_U$ ) of the structure.  $Q_{ext}$ ,  $Q_L$  and  $Q_U$  are related as [14],

$$\frac{1}{Q_L} = \frac{1}{Q_U} + \frac{1}{Q_{ext}} \quad (2.8)$$

For a bandpass resonant structure at resonant frequency with equal load and source impedances,  $Q_L$  and  $Q_U$  can be directly related by measured s-parameter values at the resonant frequency as [27],

$$Q_L = Q_U(1 - S_{21}) \quad (2.9)$$

$$Q_L = Q_U S_{11} \quad (2.10)$$

The method described so far is used to calculate the unloaded Q-factor of the inductively loaded fixed-tuned filters. The unloaded Q-factor for the end-coupled and

tapped resonator filters are approximately 140-150. This reasonably high value of Q-factor is a result of low loss in the filter and justifies the use of microstrip designs for filters in front-end receiver electronics. The loss can be further decreased by housing the filter in a metal casing such that radiation losses are minimized thus increasing unloaded Q-factor of the filter. This is especially important in microstrip circuits since they tend to have high radiation losses due to fringing fields at the edges of the microstrip line.

## CHAPTER III

## DEVELOPMENT OF THE RF MEMS SWITCH MODEL

## A. Introduction

Micro-Electro-Mechanical Systems (MEMS) are devices with dimensions in the micron range and use movable mechanical structures to control high frequency electrical signals.

RF MEMS switches are of two types: series metal-contact and shunt capacitive. The series switch makes an open circuit in the signal path when there is no bias voltage applied. When there is an actuating voltage applied, the electrostatic force developed pulls the movable membrane down to make a metal contact with the signal line thereby providing a short circuit ( $R_s < 2\Omega$ ) in the signal path. Capacitive switches make a metal-dielectric contact when an actuating voltage is applied to it resulting in a large down-state capacitance ( $C_{down} \approx 1$  pF) that provides a negligibly small impedance to the signal flowing through it. Series metal contact switches are mostly used from DC-40 GHz while capacitive switches are suitable for applications in the 10-200 GHz range. Electrostatic actuation results in the MEMS switch having a very low power consumption. Although MEMS switches have certain disadvantages such as medium switching speed (3-100  $\mu$ s) and low power handling capability ( $< 1 - 2$  V), their high linearity, low insertion loss and high isolation justify their use in RF/microwave systems which require high performance switches at relatively low speeds.

## B. Enhanced Modeling of RF MEMS Series Metal-contact Switch

Metal-contact SPST RF MEMS switches from Radant MEMS Inc. are used to implement the tunable filter. Lumped-element tunable filters in the MHz range have been designed and fabricated using this switch and they are shown to have good performance [11]. This switch has been tested to  $> 100$  billion cycles at 100 mW of RF power for  $> 100$  units [28], [29]. This section deals with the extraction of the equivalent circuit model of the packaged MEMS switch which takes all the non-idealities of the switch into account.

Fig. 19 shows the detailed structure of an eight metal-contact RF MEMS series switch from Radant MEMS Inc. The switch is made of a gold cantilever beam that is anchored at the source end and is movable at drain end. The signal flows between the drain and source connections whereas the bias voltage to the switch is applied to the gate. When an actuating voltage of 90 V or higher is applied between the gate and source electrodes, the free end of the beam is deflected and contacts the drain thus completing an electrical path between the drain and the source. Figs. 20(a),(b) show the hermetically packaged RF MEMS switch and Fig. 20(c) shows the simplified model of a series metal-contact switch. The dimensions of the fully packaged switch are  $1.42 \text{ mm} \times 1.37 \text{ mm}$ . When the switch is in the up-state (0 V) the MEMS switch is equivalent to a capacitance of 80 fF and in the down-state (90 V), the switch is equivalent to a  $0.7 \Omega$  resistor. A short high impedance transmission line on high resistivity silicon substrate is shown as a 0.15 nH inductance in series with the switch. The switch modeling methodology and its effect on filter insertion loss and bandwidth is described in detail in [11].

Fig. 21 shows the top and side views of a mounted and bond-wired RF MEMS switch on RT/Duroid substrate. The switch is mounted on top of a metallic pad

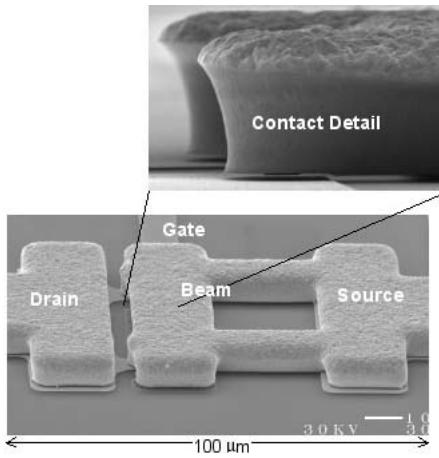


Fig. 19. Detailed structure of the RF MEMS switch from Radant MEMS Inc.

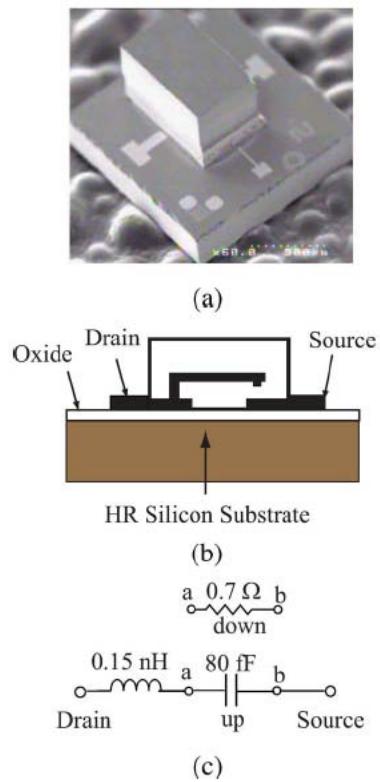


Fig. 20. (a) Photograph, (b) side view and (c) simple model of the Radant MEMS switch.

using silver epoxy. The drain, source and gate pads on the switch are  $100 \mu\text{m} \times 200 \mu\text{m}$  and they are attached by means of bond-wires to external metal landing pads ( $0.7 \text{ mm} \times 0.7 \text{ mm}$ ). The bond-wire has a length of 1 mm and a height of 0.3 mm, with a diameter of  $25 \mu\text{m}$ . Fig. 21(c) presents the enhanced circuit model considering bond-wire and mounting pad effects. The capacitance between mounting pad and RT/Duroid substrate ground is extracted from full-wave simulation using Agilent Technologies' Momentum<sup>1</sup> and fitted to a 144 fF capacitance to ground. The magnitude and phase responses between the full-wave simulation and circuit model show good agreement from 0.5-3 GHz as shown in Fig. 22. This is equivalent to a parallel plate capacitance between the landing pad and the ground plane, and can be expressed as,

$$C = C_{pp} + C_f = \frac{\epsilon_r \epsilon_0 A}{h} + C_f \quad (3.1)$$

where  $C_{pp}$  and  $C_r$  are the parallel plate and fringing capacitances respectively.  $h$  is the height of the RT/Duroid substrate and  $A$  is the area of the landing pad. The landing pad size is chosen to be  $1.9 \text{ mm} \times 1.9 \text{ mm}$  on 2.54 mm thick RT/Duroid substrate ( $\epsilon_r = 10.2$ ). The parallel plate capacitance  $C_{pp}$  is calculated to be 128 fF and the fringing field capacitance is found to be 16 fF from full-wave simulation (fringing factor,  $\gamma = 0.125$ ) resulting in a total capacitance of 144 fF.

The intrinsic switch model consists of the equivalent circuit between the switch drain and source pads through the  $2 \mu\text{m}$  thick oxide layer ( $\epsilon_r = 3.8$ ),  $250 \mu\text{m}$  thick high-resistivity silicon layer ( $\rho = 3 \text{ k}\Omega\cdot\text{cm}$ ). The intrinsic circuit depends on the switch construction alone and not on extrinsic factors such as bond-wires, mounting pads or other external parasitic effects. The intrinsic switch model has been extracted

---

<sup>1</sup>Advanced Design System (ADS) 2002A. Agilent Technologies, Palo Alto, CA, 2002.

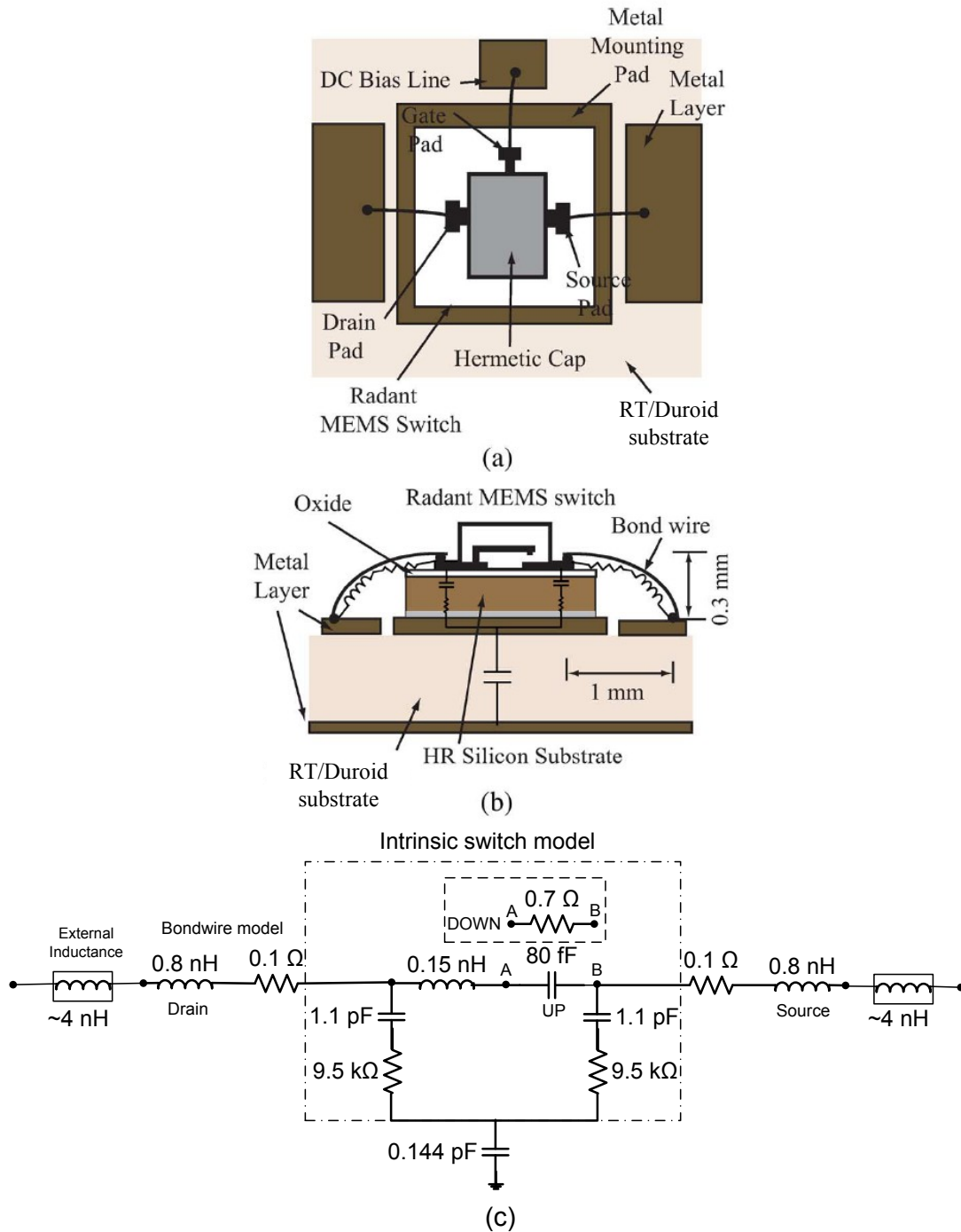
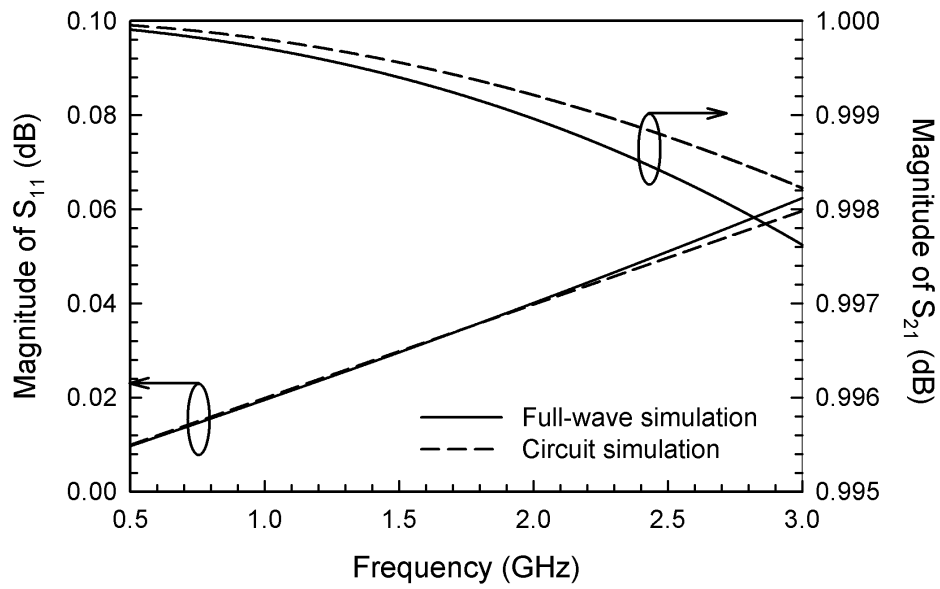
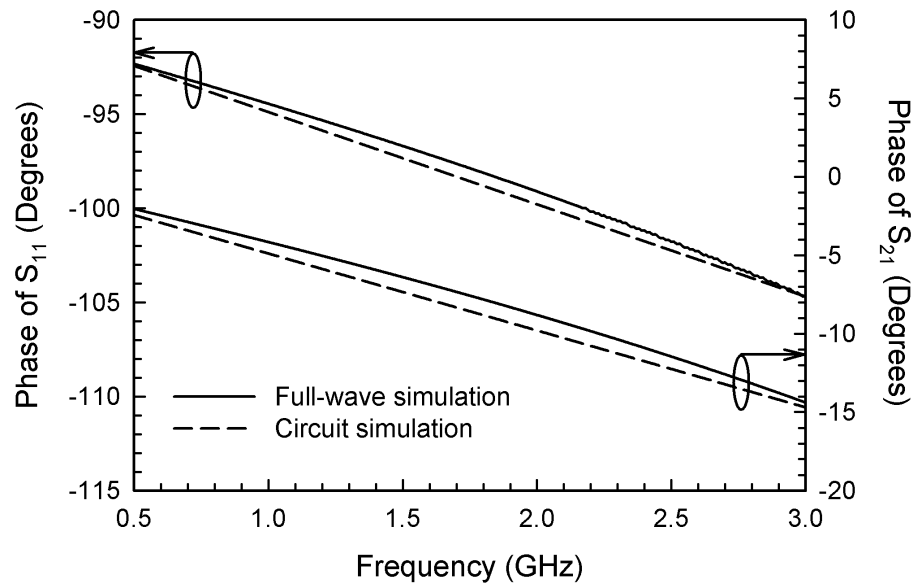


Fig. 21. (a) Top view, (b) side view, and (c) enhanced model of a mounted RF MEMS switch on RT/Duroid substrate.



(a)



(b)

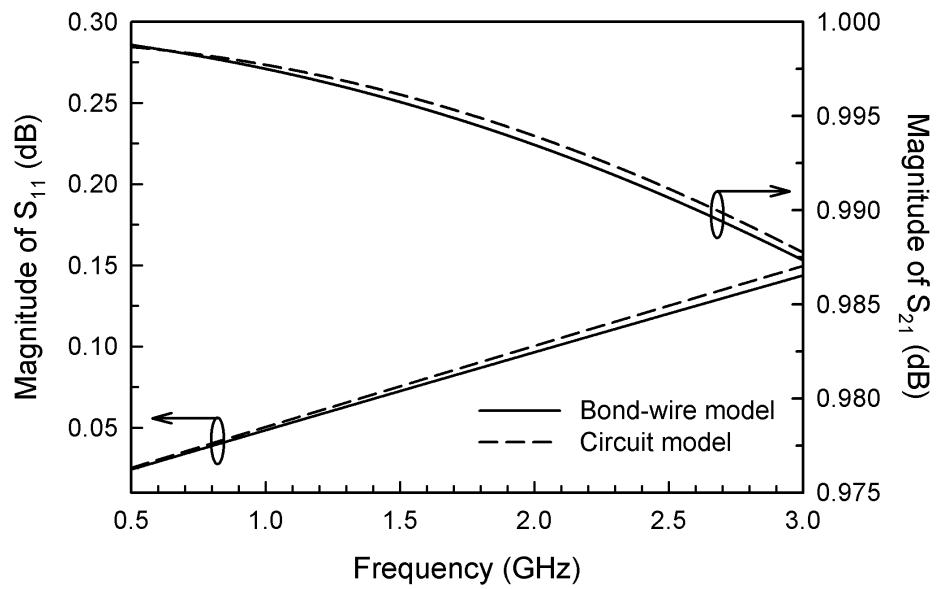
Fig. 22. (a) Simulated s-parameter magnitude response, and (b) simulated phase response of the equivalent capacitance between the switch landing pad and the RT/Duroid substrate ground.



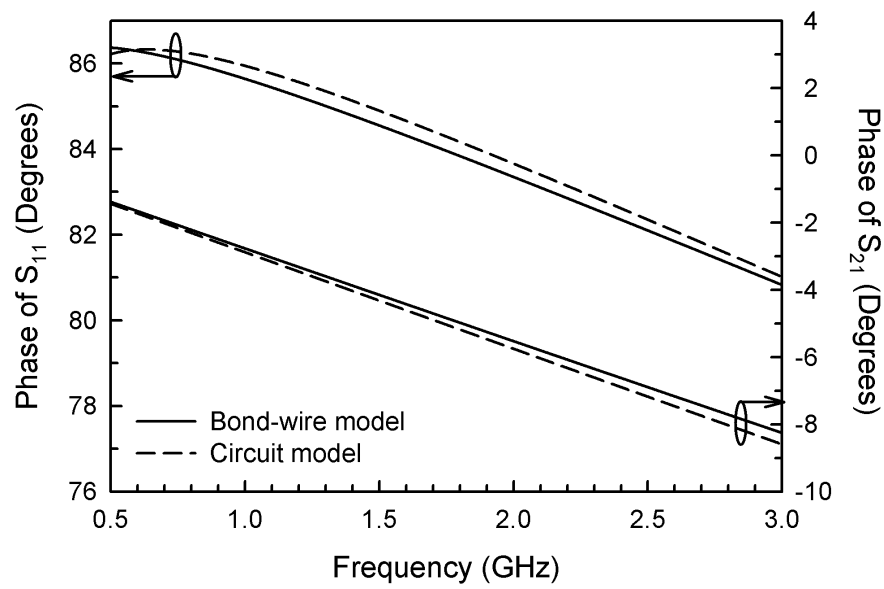
by full-wave simulation and verified by measurement in [11] for the 25-75 MHz range and remains unchanged in the 1-1.5 GHz range.

The bond-wire used to attach the MEMS switch to the rest of the filter circuit has a resistance ( $R_b$ ) and an inductance ( $L_b$ ) that is in series with the intrinsic switch model. The bond-wire is 1 mm in length and 0.3 mm in height with a diameter of 25  $\mu\text{m}$  (see Fig. 21(b)). The equivalent circuit model of the bond-wire is extracted by simulating the bond-wire model which is available in Agilent Technologies' Advanced Design System (ADS) with appropriate dimensions and then fitting it to a series R-L circuit. The comparison between bond-wire model simulation and circuit simulation is shown in Fig. 23 where the circuit simulation is the s-parameters of a series R-L circuit with  $L_b = 0.8 \text{ nH}$  and  $R_b = 0.1\Omega$ .

The transitions in the width of the microstrip line and the microstrip-bondwire transition has an equivalent inductance associated with it which is external to the switch, bond-wire and landing pads. This external inductance comes in series with the bond-wire inductance and intrinsic bridge inductance thus increasing the overall inductance in series with the switch. This inductance also depends on the exact position of the bond-wire on the bonding pad attached to the microstrip circuit and hence the accurate estimation of this inductance is a challenging task. Due to the accurate extraction of the equivalent circuits associated with the bond-wire, landing pad and the switch, an approximate estimation of the external inductance is possible by finding the value of external inductance that best emulates measured filter performance. It will be seen in chapter IV that this is in fact a valid approach due to the exact determination of all circuit elements that are a part of the tunable filter leaving the external inductance to be the only unknown factor. The results of the next chapter will also prove that the circuit model for the MEMS switch presented in this chapter predicts the filter performance accurately.



(a)



(b)

Fig. 23. (a) Simulated s-parameter magnitude response, and (b) simulated phase response of the bond-wire model and series R-L circuit with  $L_b = 0.8$  nH and  $R_b = 0.1\Omega$ .

The extracted circuit model directly affects the insertion loss and tuning range of the filter. The insertion loss arises due to the non-zero value of down-state switch resistance, conductive losses associated with the high-resistivity silicon substrate and finite conductivity of metal lines. The total series inductance of the switch which includes external inductance, bridge inductance and bond-wire inductance comes in parallel with the inductance used to tune the resonator thereby decreasing the overall loading inductance on the resonator. This significantly decreases the center frequency tuning range of the filter and also decreases the tuning range of adjustable spurious suppression. These effects will be discussed in detail in the next chapter.

## CHAPTER IV

AN INDUCTIVELY-LOADED RF MEMS TUNABLE  
FILTER WITH ADJUSTABLE SPURIOUS SUPPRESSION

## A. Introduction

Low power consumption and highly linear electrostatically actuated RF microelectromechanical systems (MEMS) switches have been extensively used in high performance miniaturized tunable microwave filters for reconfigurable RF front-ends, radar systems and wideband tracking receivers in recent years [30]. The existing solutions for RF MEMS tunable filters are based on using MEMS switches to control resonator loading. Fixed relative bandwidth over the tuning range can be achieved by employing dual coupling and loading schemes such as co-planar waveguide filters with *capacitively loaded* resonators and shunt inductive inverters [21]. An alternative topology with *inductively loaded* resonators and series capacitive inverters is necessary in microstrip designs where shunt inductive inverters are difficult to implement. Filters with dual coupling and loading schemes have a spurious passband which results in poor high frequency rejection [20]. It is possible to suppress the spurious passband for fixed filters by introducing a transmission zero to provide spurious suppression [31]. The spurious passband can be pushed to higher frequencies using distributed loading for tunable filters [21].

This chapter presents a two-pole microstrip RF MEMS tunable filter with *inductive loading* controlled by surface-mount on-chip metal-contact RF MEMS switches with electrostatic actuation. The inductive loading technique is extended to tune the spurious suppression as the filter is tuned, to achieve better rejection over the tuning range.

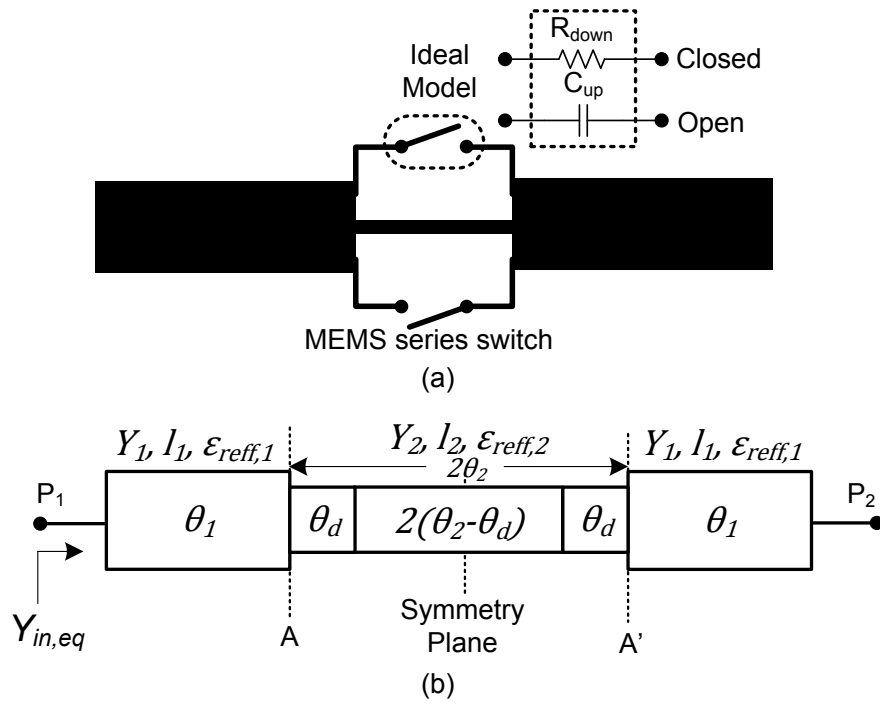


Fig. 24. (a) Proposed resonator structure, and (b) equivalent circuit of the resonator with ideal switches in the up-state position ( $Y_2 < Y_1$ ).

## B. Circuit Analysis and Design

### 1. Resonator design

The proposed half-wavelength open-ended microstrip resonator and its equivalent circuit model are shown in Fig. 24. The microstrip line step discontinuity provides an equivalent lumped inductance which is used to load the resonator. Maximum tuning is achieved when the high impedance transmission line is placed in the middle of the resonator, at the point of maximum current density. Simultaneously actuated series metal-contact RF MEMS switches are used to control the resonator loading by providing a capacitance when the switch is in the up-state position and a resistance when the switch is in the down state position. In the up-state position, the effective length of the resonator is larger and hence it provides tuning to a lower frequency. Assuming up-state switches provide an open circuit in the ideal case, the resonance condition for the loaded resonator in Fig. 24(b) can be derived by replacing the symmetry plane with an electric wall (short circuit) and solving  $Y_{in,eq} = 0$ . As a result, the resonance condition is given by,

$$\tan \theta_1 - \bar{Y}_2 \cot \theta_2 = 0 \quad (4.1)$$

where  $\theta_1$  is the electrical length corresponding to length  $l_1$  and  $\theta_2$  is corresponding to  $l_2/2$ , at filter center frequency. The bar indicates that the quantity is normalized to the admittance  $Y_1$ . Eqn. (4.1) is used to design a tunable resonator by assuming values of  $Y_1, Y_2$  and  $\theta_1$  which ensure physical realizability, and evaluating the required electrical length  $\theta_2$ . The values of  $\bar{Y}_2$  and  $\theta_2$  determine the shift in filter center frequency.  $\theta_d$  represents the equivalent shunt capacitance correction due to the step in width of the microstrip line in the resonator structure which is calculated based on formulas in [13] and then converted to its equivalent transmission line. The actual physical length

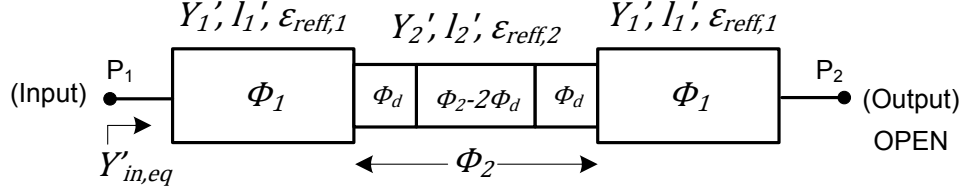


Fig. 25. Equivalent circuit of the reconfigurable open-ended stub with ideal switches in the up-state position.

of the high impedance discontinuity corresponds to an electrical length of  $2(\theta_2 - \theta_d)$  since the shunt capacitance at the discontinuity accounts for the extra length of transmission line required to meet the resonant condition. When switches are in the down-state position, the absence of a step discontinuity results in an unloaded resonator and hence a higher resonant frequency. In practice, when the switches are in the down-state position, the amount of loading inductance is never zero resulting in limited resonator tuning range. This can be included as an external inductance in series with the switch as explained in Chapter III.

## 2. Adjustable spurious suppression

The inductive loading technique is extended to design a MEMS tunable open-ended stub that is a quarter-wavelength long at the frequency of suppression. The tunable transmission zero created by the virtual short circuit at the input of the stub is used to suppress the spurious resonance. In Fig. 25, assuming ideal switches are in the up-state position, the condition for short circuit at  $P_1$  when  $P_2$  is open-ended, is  $\bar{Z}'_{in,eq} = 1/\bar{Y}'_{in,eq} = 0$  and can also be expressed as,

$$\left(\bar{Y}'_2{}^2 + 1\right) \tan \phi_2 - \bar{Y}'_2(\cot \phi_1 - \tan \phi_1) = 0 \quad (4.2)$$

The admittance  $\bar{Y}'_2$  represents the normalized admittance  $Y'_2$  of the line with length  $\phi_2$

with respect to  $Y_1'$  of the line with length  $\phi_1$  at the frequency of spurious suppression, and the prime symbols refer to reconfigurable stub parameters.  $\phi_d$  is a transmission line that accounts for the shunt capacitance in the step discontinuity. Eqn. (4.2) is used to design an adjustable stub by assuming physically realizable values of  $Y_1'$ ,  $Y_2'$  and  $\phi_1$ , and evaluating the electrical length  $\phi_2$ . The values of  $\bar{Y}_2'$  and  $\phi_2$  control the shift in the transmission zero frequency. The physical length of the high impedance discontinuity corresponds to  $\phi_2 - 2\phi_d$  since the shunt capacitance at the discontinuity accounts for the extra length of the transmission line required to meet the spurious suppression condition.

When switches are in the down-state position, the stub must effectively be quarter wavelength long at the new spurious frequency and provide a short circuit at  $P_1$ , thereby suppressing the spurious passband as the filter is tuned. As in the case of the resonator with switches in the down-state position, the equivalent loading inductance when the switches are in the down-state position is non-zero resulting in limited tuning of the transmission zero. This effect is more pronounced at higher frequencies as will be seen in the measurement of filter s-parameters.

### 3. Filter design

A two-pole 5% Chebyshev filter with 0.036-dB ripple is designed at  $f_{min} = 1.06$  GHz based on shunt resonators and J-inverters. The required values of external Q ( $Q_{ext}$ ) and inter-resonator coupling co-efficient ( $k_{12}$ ) can be found from equations 2.1, 2.2 and 2.3 which result in  $Q_{ext} = 12.64$  and  $k_{12} = 0.086$  at  $f_{min}$  as described in chapter II. The tunable open-ended stub is designed to suppress the second harmonic passband of the two-pole end-coupled microstrip filter using the resonator structure in Fig. 24 as the filter is tuned.

Fig. 26(a) shows the proposed filter layout with adjustable spurious suppression.



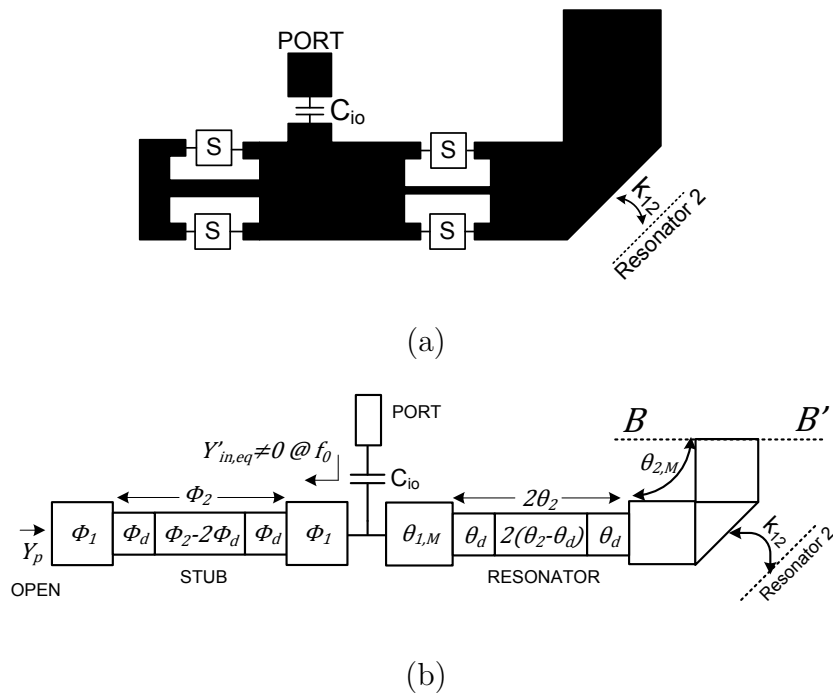


Fig. 26. (a) Proposed filter layout, and (b) equivalent half-circuit model of the filter in the up-state condition.

One arm of the resonator is bent at a right angle to achieve filter miniaturization. Each ideal MEMS switch is represented by ‘S’ and all switches are actuated simultaneously to tune the filter.  $C_{io}$  represents input/output coupling capacitance and  $k_{12}$  represents the inter-resonator mixed coupling co-efficient. The equivalent half-circuit model of the filter in the up-state condition is shown in Fig. 26(b). Since the stub input admittance is not zero at resonator center frequency ( $\bar{Y}'_{in,eq} \neq 0$  at  $f_0$ ), the new condition for resonance can be found by placing a magnetic wall (open circuit) at reference plane  $B-B'$ , neglecting coupling capacitances and finding  $\theta_{1,M}$  and  $\theta_{2,M}$  for which  $Y_p = 0$ , at resonant frequency.  $\theta_{1,M}$  and  $\theta_{2,M}$  are extracted from ADS simulations such that the new resonance condition is met. In the down-state condition, the electrical length of the overall unloaded resonator must be half wavelength long.

The circuit element values for the proposed model in Fig. 26(b) are provided in Table II. The admittance values are chosen as  $Y_1 = Y'_1 = 1/30$  S,  $Y_2 = 1/100$  S and  $Y'_2 = 1/75$  S and electrical lengths related to the resonator are at  $f_{min}$ , while those related to the stub are at  $2f_{min}$ . Fig. 27 shows the circuit simulation results in ADS for the case when all the switches are in the up-state and it is seen that the passband is at 1.06 GHz while the harmonic frequency at 2.12 GHz is suppressed by the open-ended quarter-wavelength stub. The filter layout is simulated using SONNET and tabulated electrical lengths are mapped into their corresponding physical lengths after full-wave simulation. The input/output capacitance value and inter-resonator gap length are also found by full-wave simulation using the methodology described in [13].

Table II. Tunable Filter Model Element Values ( $Y_1 = Y'_1 = 1/30$  S,  $Y_2 = 1/100$  S,  $Y'_2 = 1/75$  S)

$\theta_{1,M}$	20.4°	$\theta_{2,M}$	38.7°	$\theta_2$	13.5°	$\theta_d$	10.8°
$\phi_1$	11.8°	$\phi_2$	57.8°	$\phi_d$	14°	-	-

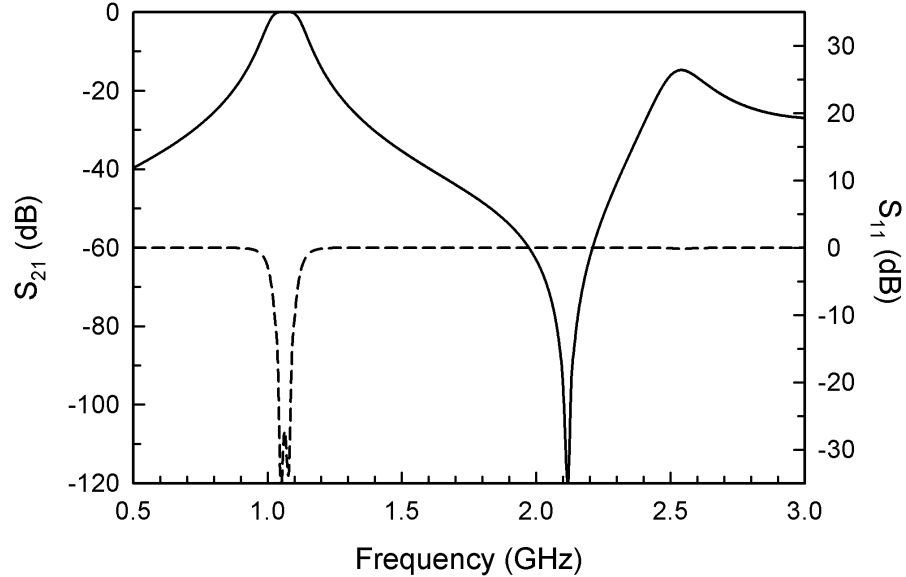


Fig. 27. Circuit simulation of the tunable filter with adjustable harmonic suppression when all the switches are in the up-state position.

The ideal series RF MEMS switch is replaced by a packaged metal contact switch from Radant MEMS Inc. The enhanced MEMS switch model shown in Fig. 21(c) in chapter III is discussed in detail in [11]. The intrinsic switch model remains the same as in [11] but the bond wire inductance and landing pad capacitance are recalculated for RT/Duroid substrate between 0.5 to 3 GHz. The changes in microstrip line width around the MEMS switch and the transition from microstrip line to bond wire results in an additional external inductance which is in series with the switch. Full-wave simulation results for the tunable filter using the enhanced switch model are discussed in section C.

### C. Fabrication and Measurement

The microstrip filter is fabricated on RT/Duroid 6010LM substrate with  $\epsilon_r = 10.2 \pm 0.25$ ,  $\tan \delta = 0.0023$  and thickness of 2.54 mm clad with  $35 \mu\text{m}$  electrodeposited

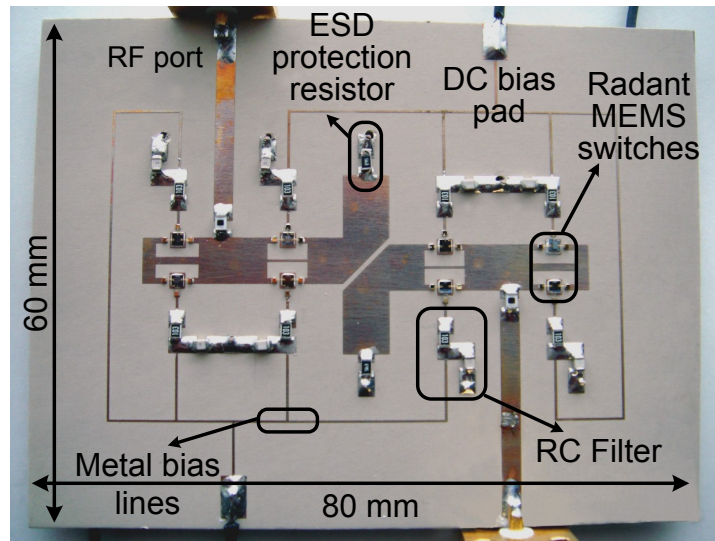
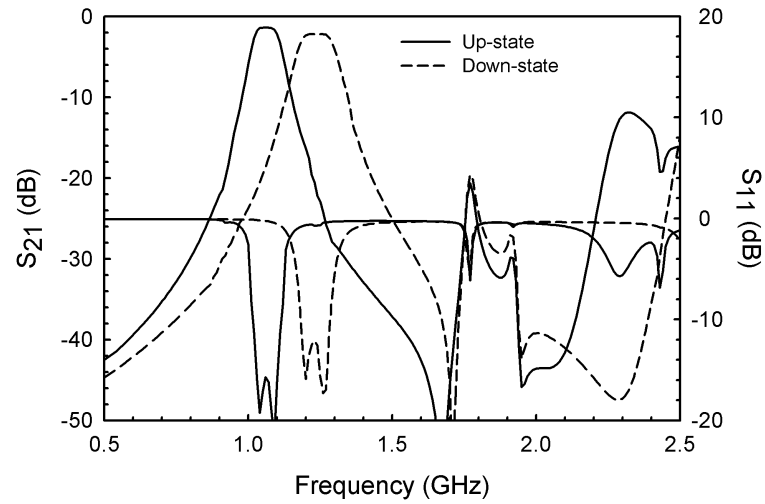


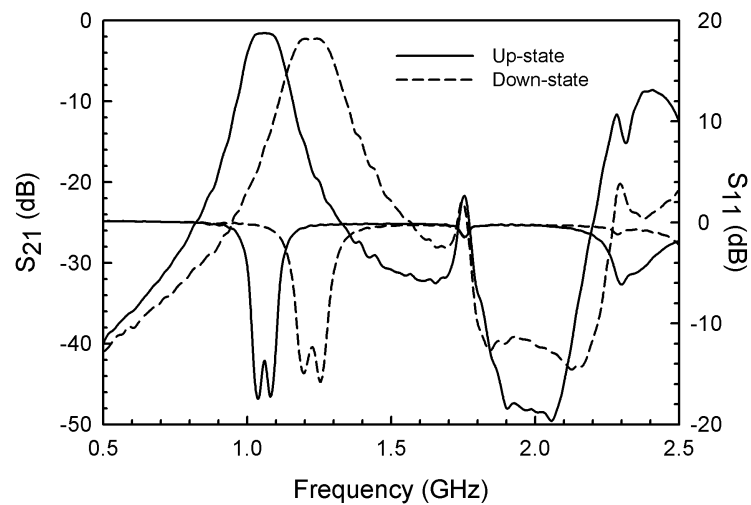
Fig. 28. Photograph of the fabricated RF MEMS tunable filter.

copper. The filter is excited using  $50\Omega$  input/output microstrip lines. The input/output J-inverter capacitances ( $C_{io} = 2.2$  pF) are provided by discrete thin-film surface mount capacitors, and the inter-resonator mixed coupling coefficient ( $k_{12}$ ) is implemented with a gap of 0.8 mm. The switch actuation voltage (90 V) is applied to the gate of the switch using copper bias lines. Each resonator has a  $56$  k $\Omega$  resistor connected to ground to prevent any DC floating nodes across the switch, which could result in electrostatic discharge. Each switch has a separate DC coupling R-C filter ( $R = 10$  k $\Omega$ ,  $C = 10$  pF,  $f_c = 1.6$  MHz) for added isolation between DC and RF signals.

Fig. 28 shows the fabricated filter and Fig. 29 shows the simulated and measured filter performances. The enhanced switch model is included in full-wave simulations for up-state and down-state conditions. The filter shows center frequencies of 1.06 GHz to 1.23 GHz when switches are in the up-state and down-state position respectively. The insertion loss changes from 1.56 dB to 2.28 dB with return loss better than 13 dB over the tuning range while the measured unloaded Q of the filter changes from



(a)



(b)

Fig. 29. (a) Simulated filter s-parameters with switches in up-state and down-state positions including the effect of enhanced switch model. (b) Measured filter performance for two different states.

127 to 75. The 4 nH external inductance in series with the switch limits the tuning range of the filter. This effect is more significant at higher frequencies resulting in limited tuning of the adjustable stub. Reducing the external inductance to 1 nH by tapering switch drain/source landing pads and using parallel bond wires will result in 8.5% improvement in the passband tuning range and wider suppression tuning. The presence of a spike at 1.74 GHz for both filter states is due to an unwanted coupling path from the input to the output of the filter through metal bias lines on the substrate. The rejection performance can be improved by providing a separate bias pad to each switch and also by adding extra RC filters on different locations of the metal bias path to suppress any RF leakage through the biasing circuitry.

#### D. Fundamental Limitations in Filter Tuning

The fundamental limits on the frequency tuning range of the filter is determined by constraints imposed in the physical realization of the tunable filter. The resonator center frequency is directly related to the amount of loading inductance provided by the step-discontinuity in the microstrip line whose ratio of line widths is determined by ‘ $r$ ’. The maximum shift in resonator frequency is dependent upon the lowest achievable value of ‘ $r$ ’ by the fabrication processes involved.

The next fundamental limitation on the tuning range of the filter is related to the maximum allowable mismatch at the filter input/output. In order to maintain a constant return loss as the resonators in the filter are tuned, it is necessary to tune all the inverters present in the filter structure. To achieve such a completely tunable structure is challenging and often cumbersome, and its need is entirely based on the filter application. In filters with constant inverters and tunable resonators, the mismatch increases as the filter is tuned to lower frequencies, leaving the tuning

range to be limited by the maximum allowable mismatch in the system.

Apart from these limitations, parasitic inductances and capacitances associated with hybrid microwave structures play an important role in estimating the maximum achievable system performance. For the filter described in this chapter, the parasitic inductances and capacitances associated with microstrip transitions, bond-wires, RF MEMS switch and connectors have a direct effect on the overall resonator loading, and in turn impose a restriction on the tunability of the microwave filter. Among these limiting factors, the external inductance (4 nH) is the most significant one and contributes to approximately 10% reduction in tuning range. Bond-wire inductance and bridge inductance do not contribute significantly to reduction in filter tuning range.

## CHAPTER V

## CONCLUSION AND FUTURE WORK

## A. Conclusion

The main purpose of this thesis is the development of RF MEMS tunable filters for use in low-power, reconfigurable front-end systems. The first part of this thesis deals with the design, simulation, fabrication and measurement of fixed-tuned microstrip filters with inductive loading. By introducing a step-discontinuity in a half-wavelength microstrip resonator, it has been shown that the resonance is moved to lower frequencies. The presence of a spurious upper passband in microwave filters with inductive-loading and capacitive coupling, such as those presented in this thesis, degrades the upper rejection skirt. The method of tapped resonator loading has been applied to suppress the spurious resonance and improve the upper rejection performance. Both end-coupled and tapped resonator filters have center frequencies of 1.36 GHz and 1.03 GHz in the unloaded and loaded state respectively. The insertion losses of these filters are relatively low and are measured to be between 1.2-1.5 dB, with return loss better than 10 dB for all fixed-tuned filters. The measured unloaded quality factor for the fixed filters are between 140-150.

The second part of this thesis deals with the electromagnetic modeling of the RF MEMS switch developed by Radant MEMS Inc., in the 1-1.5 GHz range. The equivalent switch model is extracted considering the effects of mounting pads, bond-wires and other external parasitics due to discontinuities in the microstrip structure. Full-wave electromagnetic and circuit simulations have been matched to good agreement to derive the enhanced RF MEMS switch model. This model is used in the design of the RF MEMS tunable filter and accurately predicts the filter performance.



The last part of this thesis deals with the design, fabrication and testing of the RF MEMS tunable filter. The inductive loading mechanism used to tune the resonator is extended to tune the open-ended stub, resulting in tunable second harmonic suppression. To our knowledge, this is the first demonstration of tunable spurious suppression in planar microwave filters. The filter has center frequencies of 1.23 GHz and 1.06 GHz, with insertion losses of 1.56 dB and 2.28 dB when the switches are in the down-state and up-state position respectively. It is seen that the insertion loss when the switch is in the up-state remains relatively the same as the fixed filter, implying that the dominant loss mechanism is the metallic and dielectric losses associated with the microstrip structure. The RF MEMS switch loss is significant when the switches are in the down-state due to the switch resistance resulting in higher filter loss. The measured return losses are better than 13 dB in both filter states. The measured unloaded quality factor is 127 and 75 when the switches are in the up-state and down-state positions respectively. In the down-state position, the down-state bridge resistance increases the loss of the filter resulting in lower Q factor. The measured filter response shows an unwanted spike at 1.74 GHz due to a stray coupling path between the input and the output through the metal bias lines on the substrate. The second harmonic resonance has been suppressed below -20 dB and is limited by the constant spike at 1.74 GHz. The absence of this spike would result in approximately 40 dB of spurious suppression. Methods to reduce this stray coupling has been explained and techniques to improve the tuning range of the filter has been proposed.

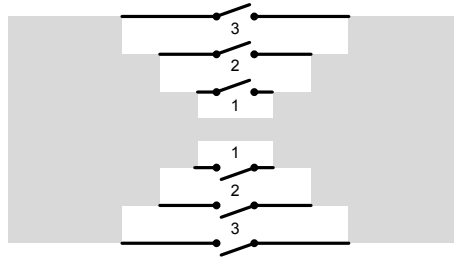


Fig. 30. Inductive loading section for multi-state tunable filter.

## B. Future Work

### 1. Multi-bit tunable filter

The two-state tunable filter described in this thesis can be extended to higher number of tunable filter states, thus resulting in a contiguously tunable filter. Such a tunable filter will provide higher resolution over the frequency band being selected which is important in wideband reconfigurable front-end systems. The inductive loading section for a tunable resonator with three switches is shown in Fig. 30. When all the switches are in the up-state position, the inductive loading is maximum and hence the resonator is tuned to the lowest frequency. By closing switches 1, 2 and 3 one by one, the equivalent loading inductance decreases thus tuning the filter to higher frequencies. With this structure, a total of four filter states can be achieved. For higher number of filter states, the fabrication of the filter with discrete packaged MEMS switches becomes increasingly cumbersome. To overcome this problem, the RF MEMS switches must be fabricated monolithically with the microstrip filter thus providing extremely small tunable elements that can be incorporated into the tunable filter.

## 2. Millimeter-wave RF MEMS tunable filter

The filter described in this thesis can be extended to design a millimeter-wave tunable filter, for example at 24 and 31 GHz for wireless high data-rate applications in Industrial, Scientific and Medical (ISM) frequency bands and Local Multi-point Distribution Systems (LMDS). Fig. 31 shows a tunable filter for the 24-31 GHz range using embedded shunt RF MEMS capacitive switches in end-coupled half-wavelength microstrip resonators on 500  $\mu\text{m}$  thick glass substrate. RF MEMS shunt capacitive switches provide excellent performance at millimeter-wave frequencies and can be used to control the resonator loading to achieve tuning. The suspended movable membranes in MEMS capacitive switches are typically formed using a sputtered Ti/Au layer and released using critical point drying. The MEMS bridge dimensions are 160  $\mu\text{m}$   $\times$  100  $\mu\text{m}$  and is suspended at a height of 1.5  $\mu\text{m}$  above a silicon nitride dielectric layer. The MEMS bridge is actuated using an electrostatic potential between the bottom electrode and the bridge itself. The performance of such a filter is excellent due to the low loss, high isolation and high linearity of RF MEMS capacitive switches. The parasitics associated with packaged RF MEMS switches are absent in this case because the switches are monolithically fabricated along with the filter and enables wide range of filter tuning. Fig. 32 shows the full wave filter simulation using Sonnet. The filter loss is estimated to be around 2.1-2.5 dB at the two center frequencies. The spurious resonant passband occurs at 39 GHz when the switches are in the up-state position and results in poor rejection at frequencies higher than the filter center frequency. The spurious suppression methodology developed in chapter IV of this thesis can be used to reject the spurious resonance and improve the high frequency rejection of the tunable filter.

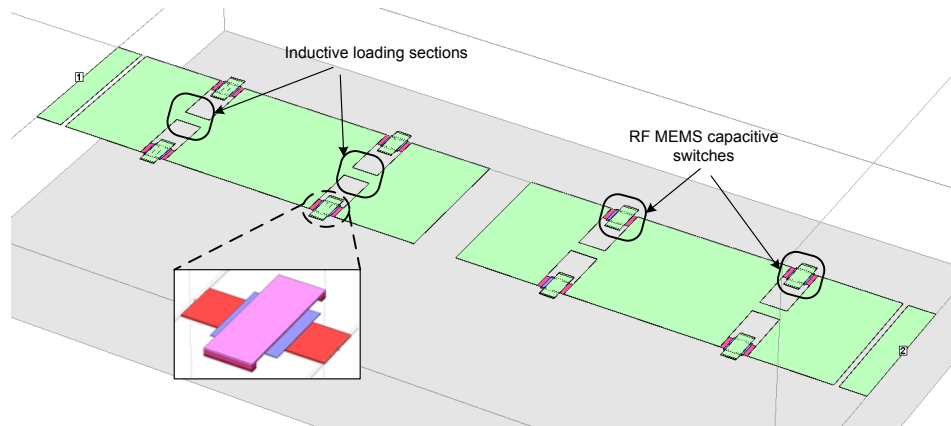


Fig. 31. Millimeter-wave RF MEMS tunable filter for 24-31 GHz applications.

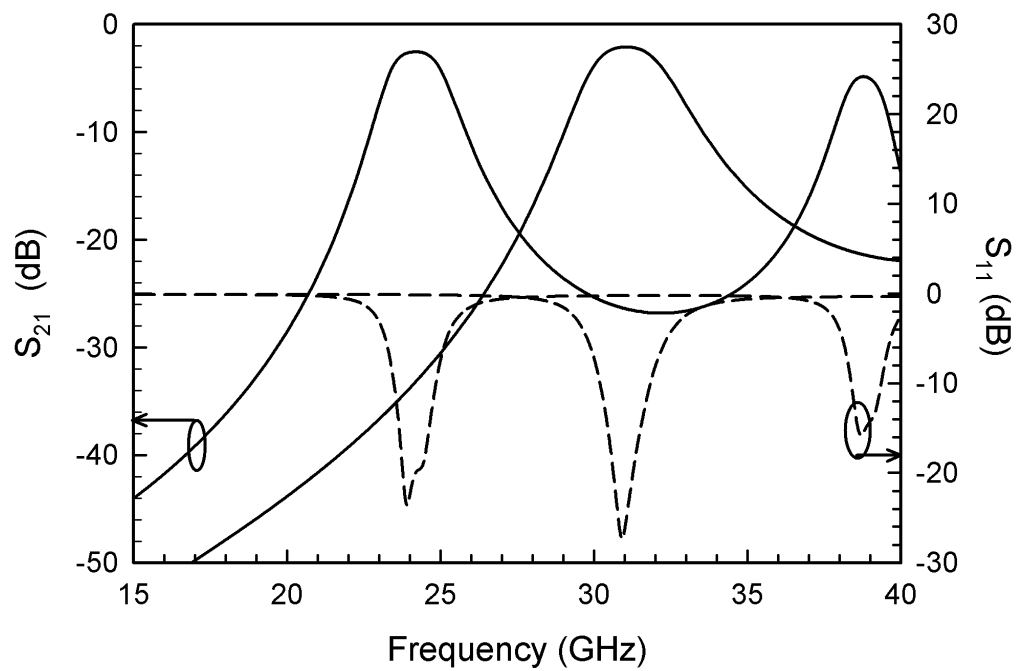


Fig. 32. Simulated results of the 24-31 GHz RF MEMS tunable filter.

## REFERENCES

- [1] I. C. Hunter, L. Billonet, B. Jarry and P. Guillan, "Microwave filters - applications and technology," *IEEE Transactions on Microwave Theory and Techniques*, vol. 50, pp. 794-805, March 2002
- [2] J. Uher and W. J. R. Hoefer, "Tunable microwave and millimeter-wave band-pass filters," *IEEE Transactions on Microwave Theory and Techniques*, vol. 39, no. 4, pp. 643-653, Apr 1991
- [3] M. A. Kunes and G .G. Connor, "A digitally controlled tunable, high output filter for space applications," *in Proc. 19th European Microwave Conference*, pp. 681-686, Oct. 1989
- [4] H. Tanbakuchi, D. Nicholson, B. Kunz and W. Ishak, "Magnetically tunable oscillators and filters" *IEEE Transactions on Magnetics* , vol. 25, no. 5, pp. 3248-3253, September 1989
- [5] Y. Murakami, T. Ohgihara and T. Okamoto, "A 0.5-4.0-GHz tunable bandpass filter using YIG film grown by LPE," *IEEE Transactions on Microwave Theory and Techniques*, vol. 35, no. 12, pp. 1192-1198, Dec 1987
- [6] B. -W. Kim and S. -W. Yun, "Varactor-tuned combline bandpass filter using step-impedance microstrip lines," *IEEE Transactions on Microwave Theory and Techniques*, vol. 52, no. 4, pp. 1279-1283, April 2004
- [7] A. Eriksson, A. Deleniv, S. Gevorgian, B. Lumetzberger and N. Billstrom, "GaAs varactor tuned filter for low power applications," *in 2005 IEEE MTT-S International Microwave Symposium Digest*, pp. 2211-2214, June 2005

- [8] J. Nath, D. Ghosh, J. P. Maria, A. I. Kingon, W. Fathelbab *et al.*, “An electronically tunable microstrip bandpass filter using thin-film Barium-Strontium-Titanate (BST) varactors,” *IEEE Transactions on Microwave Theory and Techniques*, vol. 53, no. 9, pp. 2707-2712, September 2005
- [9] J. Muldavin, C. O. Bozler, S. Rabe, P. W. Wyatt and C. L. Keast, “Wafer-scale packaged RF microelectromechanical switches,” *IEEE Transactions on Microwave Theory and Techniques*, vol. 56, no. 2, pp. 522-529, Feb. 2008
- [10] B. Pillans, A. Malczewski, R. Allison and J. Brank, “6-15 GHz RF MEMS tunable filters,” in *2005 IEEE MTT-S International Microwave Symposium Digest*, pp. 4, 12-17 June 2005
- [11] K. Entesari, K. Obeidat, A. R. Brown and G. M. Rebeiz, “A 25-75 MHz RF MEMS tunable filter,” *IEEE Transactions on Microwave Theory and Techniques*, vol. 55, no. 11, pp. 2399-2405, Nov. 2007
- [12] E. R. Brown, “RF-MEMS switches for reconfigurable integrated circuits,” *IEEE Transactions on Microwave Theory and Techniques*, vol. 46, no. 11, pp. 1868-1880, Nov 1998
- [13] J. S. Hong and M. J. Lancaster, *Microstrip Filters for RF/Microwave Applications*. New York: Wiley, 2001
- [14] G. L. Matthaei, E. Young and E. M. T. Jones, *Microwave Filters, Impedance-matching Networks and Coupling Structures*. Norwood, MA: Artech House, 1980
- [15] S. B. Cohn, “Direct-coupled resonator filters,” *Proceedings of the IRE*, vol. 45, no. 2, pp. 187-196, Feb. 1957

- [16] S. B. Cohn, "Parallel-coupled transmission-line resonator filters," *IEEE Transactions on Microwave Theory and Techniques*, vol. 6, no. 2, pp. 223-231, Apr 1958
- [17] M. Dishal, "Alignment and adjustment of synchronously tuned multiple-resonant-circuit filters," *Proceedings of the IRE*, vol. 39, no. 11, pp. 1448-1455, Nov. 1951
- [18] D. G. Swanson, "Narrow-band microwave filter design," *IEEE Microwave Magazine*, vol. 8, no. 5, pp. 105-114, Oct. 2007
- [19] J. -S. Hong and M. J. Lancaster, "Couplings of microstrip square open-loop resonators for cross-coupled planar microwave filters," *IEEE Transactions on Microwave Theory and Techniques*, vol. 44, no. 11, pp. 2099-2109, Nov 1996
- [20] A. Abbaspour-Tamijani, "Novel components for integrated millimeter-wave front ends," *Ph.D Dissertation*, The University of Michigan, Ann Arbor, MI, 2004
- [21] A. Abbaspour-Tamijani, L. Dussopt and G. M. Rebeiz, "Miniature and tunable filters using MEMS capacitors," *IEEE Transactions on Microwave Theory and Techniques*, vol. 51, no. 7, pp. 1878-1885, July 2003
- [22] K. Entesari and G. M. Rebeiz, "A 12-18-GHz three-pole RF MEMS tunable filter," *IEEE Transactions on Microwave Theory and Techniques*, vol. 53, no. 8, pp. 2566-2571, Aug. 2005
- [23] J. -T. Kuo, S. -P. Chen and M. Jiang, "Parallel-coupled microstrip filters with over-coupled end stages for suppression of spurious responses," *IEEE Microwave and Wireless Components Letters*, vol. 13, no. 10, pp. 440-442, Oct. 2003

- [24] Md. C. Velazquez-Ahumada, J. Martel and F. Medina, "Parallel coupled microstrip filters with ground-plane aperture for spurious band suppression and enhanced coupling," *IEEE Transactions on Microwave Theory and Techniques*, vol. 52, no. 3, pp. 1082-1086, March 2004
- [25] S.-M. Wang, C.-H. Chi, M.-Y. Hsieh, and C.-Y. Chang, "Miniaturized spurious passband suppression microstrip filter using meandered parallel coupled lines," *IEEE Transactions on Microwave Theory and Techniques*, vol. 53, no. 2, pp. 747-753, Feb. 2005
- [26] J. S. Wong, "Microstrip tapped-line filter design," *IEEE Transactions on Microwave Theory and Techniques*, vol. 27, no. 1, pp. 44-50, Jan 1979
- [27] A. R. Brown, "High-Q integrated micromachined components for a 28 GHz front-end transceiver," *Ph.D Dissertation*, The University of Michigan, Ann Arbor, MI, 1999
- [28] J. Lampen, S. Majumder, R. Morrison, A. Chaudhry and J. Maciel, "A wafer-capped, high-lifetime ohmic MEMS RF switch," *International Journal of RF and Microwave Computer-Aided Engineering*, vol. 14, pp. 338-344, Jul. 2004
- [29] S. Majumder, J. Lampen, R. Morrison and J. Maciel, "A packaged, high-lifetime ohmic MEMS RF switch," in *IEEE MTT-S International Microwave Symposium Digest*, pp. 1935-1938, Jun. 2003
- [30] G. M. Rebeiz, *RF MEMS Theory, Design and Technology*. New York: Wiley, 2003
- [31] J.-T. Kuo and E. Shih, "Microstrip stepped impedance resonator bandpass filter with an extended optimal rejection bandwidth," *IEEE Transactions on*



*Microwave Theory and Techniques*, vol. 51, no. 5, pp. 1554-1559, May 2003

## VITA

Vikram Sekar received his Bachelor of Engineering degree in telecommunications from R. V. College of Engineering, Bangalore under the Visveswariah Technological University. During the final year of his undergraduate program, he worked on reconfigurable microstrip antennas for mobile vehicular systems. He started pursuing his master's degree in electrical engineering at Texas A&M University under the guidance of Dr. Kamran Entesari in August 2006. His research interests include frequency-agile microwave circuits, metamaterials, synthesis of electrical networks and electromagnetic theory. Vikram's permanent address is No. 14, "Surabhi", Baroda Bank Colony, 5th main, Puttenahalli, J.P. Nagar 7th Phase, Bangalore-560078, India.